https://doi.org/10.1093/plcell/koad257 THE PLANT CELL 2023: 1–25

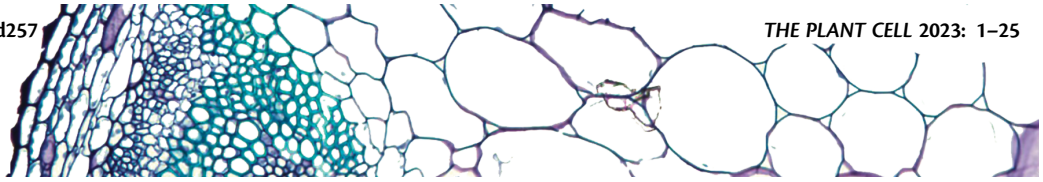

Research Article

The cytokinin receptor OHK4/OsHK4 regulates inflorescence architecture in rice via an IDEAL PLANT ARCHITECTURE1/WEALTHY FARMER'S PANICLE-mediated positive feedback circuit

Yan Chun, Jingjing Fang, Ekaterina M. Savelieva, Sergey N. Lomin, Jiangyuan Shang, Yinglu Sun, Jinfeng Zhao, Ashmit Kumar, Shoujiang Yuan, Xuefeng Yao, Chun-Ming Liu, Dmitry V. Arkhipov, Georgy A. Romanov* and Xueyong Li*

*Author for correspondence: lixueyong@caas.cn (X.L.), gar@ippras.ru (G.A.R.)
†These authors contributed equally.
The author responsible for distribution of materials integral to the findings presented in this article in accordance with the policy described in the Instructions for Authors (https://academic.oup.com/plcell/pages/General-Instructions) is: Xueyong Li (lixueyong@caas.cn).

Abstract

Inflorescence architecture is important for rice (*Oryza sativa*) grain yield. The phytohormone cytokinin (CK) has been shown to regulate rice inflorescence development; however, the underlying mechanism mediated by CK perception is still unclear. Employing a forward genetic approach, we isolated an inactive variant of the CK receptor *OHK4*/*OsHK4* gene named *panicle length1*, which shows decreased panicle size due to reduced inflorescence meristem (IM) activity. A 2-amino acid deletion in the long α-helix stalk of the sensory module of OHK4 impairs the homodimerization and ligand-binding capacity of the receptor, even though the residues do not touch the ligand-binding domain or the dimerization interface. This deletion impairs CK signaling that occurs through the type-B response regulator OsRR21, which acts downstream of OHK4 in controlling inflorescence size. Meanwhile, we found that *IDEAL PLANT ARCHITECTURE1*(*IPA1*)/*WEALTHY FARMER'S PANICLE* (*WFP*), encoding a positive regulator of IM development, acts downstream of CK signaling and is directly activated by OsRR21. Additionally, we revealed that IPA1/WFP directly binds to the *OHK4* promoter and upregulates its expression through interactions with 2 TCP transcription factors, forming a positive feedback circuit. Altogether, we identified the OHK4-OsRR21-IPA1 regulatory module, providing important insights into the role of CK signaling in regulating rice inflorescence architecture.

Introduction

Rice (*Oryza sativa*) yield is closely associated with inflorescence architecture, which consists of panicle length, primary and secondary branch number, as well as grain number per panicle. Inflorescence architecture is largely determined by meristem activity (Li et al. 2013; Chun et al. 2022). In recent years, several genes regulating rice meristem activity and ultimately affecting inflorescence architecture have been characterized, such as *CLASS I KNOTTED1-LIKE HOMEOBOX* (*KNOX1*), *LAX PANICLE1* (*LAX1*), *LAX2*, *ABERRANT PANICLE ORGANIZATION1* (*APO1*), *APO2*/*RICE FLORICAULA* (*RFL*), and *ABERRANT SPIKELET AND PANICLE1* (*ASP1*) (Komatsu et al. 2001, 2003; Ikeda et al. 2005; Rao et al. 2008; Ikeda-Kawakatsu et al. 2009; Tabuchi et al. 2011; Tsuda et al. 2011; Ikeda-Kawakatsu et al. 2012; Yoshida et al. 2012). Loss of function of these genes usually leads to reduced activity of the shoot apical meristem (SAM) or axillary meristem, leading to the formation of panicles with reduced length, fewer branches, and fewer spikelets (Kurakawa et al. 2007). On the other hand, an enhancement of meristem activity may generate larger panicles and increase grain

Received March 01, 2023. Accepted August 18, 2023. Advance access publication October 9, 2023

IN A NUTSHELL

Background: The plant hormone cytokinin (CK) promotes plant meristem initiation and maintenance. A high level of CK in rice can enhance meristem activity and enlarge panicles, while a low level of CK can cause premature termination of the meristem and result in smaller panicles. The CK signal is transmitted from histidine kinase (HK) receptors to phosphotransfer proteins (HPts) and response regulators (RRs). The roles of several CK receptors and RRs in rice panicle development have been partially revealed, but their regulatory relationships and downstream factors remain unclear.

Question: Which RR receives the CK signal from the CK receptor OHK4? Which genes controlling panicle size are influenced by RRs? Are there any regulators that affect OHK4?

Findings: We discovered that a loss-of-function mutation of *OHK4* disrupts CK signaling and reduces rice panicle size. The phosphorylation level of the type-B RR OsRR21 is dependent on OHK4. Overexpression of *OsRR21* partially rescued the short panicle phenotype of the *ohk4* mutant. *IDEAL PLANT ARCHITECTURE1 (IPA1)/WEALTHY FARMER'S PANICLE (WFP)*, encoding a positive regulator of rice panicle size, is directly activated by OsRR21. Interestingly, *OHK4* expression is upregulated in the gain-of-function mutant *ipa1-D* but downregulated in loss-of-function *ipa1* mutants. Genetic and molecular analyses revealed that IPA1/WFP regulates *OHK4* through interactions with 2 TCP transcription factors. Therefore, OHK4, OsRR21, and IPA1/WFP form a positive feedback loop to control meristem activity and panicle development in rice.

Next steps: Although the connection between OHK4 and OsRR21 has been revealed, we still do not know which histidine HPts act as intermediates in this process. The relationship between OHK4 and other RRs is also not clear. Whether OsRR21 regulates other meristem or inflorescence regulators is quite an intriguing issue.

yield (Huang et al. 2009). Overexpression of *RICE CENTRORADIALIS1* (*RCN1*) and *RCN2* produces more panicle branches and spikelets, probably due to the delayed transition of an active meristem to a specific meristem (Nakagawa et al. 2002). The gain-of-function allele of *DENSE AND ERECT PANICLE1* (*DEP1*) enhances SAM activity, resulting in increased grain number (Huang et al. 2009). *TAWAWA1* (*TAW1*) positively regulates inflorescence meristem (IM) activity, as the gain-of-function mutant *tawawa1-D* generates increased numbers of panicle branches and spikelets due to prolonged IM activity (Yoshida et al. 2013). *IDEAL PLANT ARCHITECTURE1* (*IPA1*)/*WEALTHY FARMER'S PANICLE* (*WFP*), encoding the transcription factor SQUAMOSA PROMOTER BINDING PROTEIN-LIKE 14 (OsSPL14), is another regulator of IM activity. Gain-of-function alleles of *OsSPL14* with the optimal expression levels such as $OsSPL14^{IPA1}$ and $OsSPL14^{WFP}$ produce more spikelets than the wild type (WT) (Jiao et al. 2010; Miura et al. 2010), while excessive levels of OsSPL14 led to reduced numbers of spikelets (Wang et al. 2015).

The phytohormone cytokinin (CK) plays a critical role in determining meristem activity. The accumulation of endogenous CKs can enhance meristem activity and crop productivity. For example, downregulating *GRAIN NUMBER1a* (*Gn1a*), which encodes a CK oxidase/dehydrogenase, increases panicle branch number and grain yield due to increased CK contents in IMs (Ashikari et al. 2005). Conversely, a loss-of-function mutation of *LONELY GUY* (*LOG*), which encodes a CK-activating enzyme, caused premature termination of IMs and small panicles (Kurakawa et al. 2007). The effect of CKs on inflorescences is also indirectly regulated by other genes, such as *DROUGHT AND SALT TOLERANCE* (*DST*), *LARGER PANICLE* (*LP*), and *VIN3-LIKE 2* (*OsVIL2*), which affect CK accumulation and inflorescence architecture through regulating the expression of *Gn1a* (Li et al. 2011; Li et al. 2013; Yang et al. 2019).

CK perception in plants is mediated by a two-component system (TCS) containing a histidine kinase (HK) that receives the input signal and a response regulator (RR) that usually acts as a transcription factor that is activated in response to the CK signal. In *Arabidopsis* (*Arabidopsis thaliana*), the CK receptors AHK2, AHK3, and CRE1/AHK4 were identified, and their functions in plant development were extensively studied (Inoue et al. 2001; Higuchi et al. 2004; Nishimura et al. 2004; Kim et al. 2006; Riefler et al. 2006; Stolz et al. 2011; Chang et al. 2013; Bartrina et al. 2017). Notably, the *ahk2 ahk3 ahk4* triple mutant produces a dramatically small SAM with reduced numbers of cell layers and fewer cells per layer than the WT (Higuchi et al. 2004; Nishimura et al. 2004; Riefler et al. 2006). The CK receptors OHK2/OsHK3, OHK3/OsHK5, OHK4/OsHK4, and OHK5/OsHK6 were identified in rice (Ito and Kurata 2006; Choi et al. 2012). In addition, an unusual CK receptor (CHARK) from rice exhibiting non-histidine but serine/threonine kinase activity was recently characterized (Halawa et al. 2021). However, only a few CK receptor mutants have been reported. A missense mutation in *OHK5*/*OsHK6* enhances the root tolerance to CK but causes no obvious effects on other morphologies (Ding et al. 2017). The functions of *OHK3*/*OsHK5* and *OHK5*/*OsHK6* were recently characterized by reverse genetics (Burr et al. 2020). Similar to their putative orthologs, *OHK3*/*OsHK5* and *OHK5*/*OsHK6* play overlapping roles in controlling multiple aspects of rice development, such as root growth, leaf width, and inflorescence architecture. Nevertheless, the

entire spectrum of the effects of CK receptors in regulating rice biology, especially meristem activity, remains largely unknown.

In this study, we characterized the rice mutant *panicle length1* (*pal1*), which shows reduced panicle size and grain yield due to the downregulation of IM activity. Our analyses suggested that this mutation impairs the homodimerization and ligand-binding capacity of the CK receptor OHK4. We found that the activity of the type-B RR OsRR21 is dependent on *OHK4*. OsRR21 directly regulates *IPA1*, and in turn, IPA1 regulates *OHK4* expression via interactions with 2 TCP transcription factors, forming a positive feedback circuit. Overall, our study identified the OHK4-OsRR21-IPA1 regulatory module, which substantially affects rice inflorescence architecture by regulating meristem activity and consequently determines grain yield.

Results

Morphological characterization of the *pal1* mutant

Compared with WT (*japonica* variety 'Huaidao 5') rice, the *pal1* mutant generated shorter panicles with a reduced number of primary and secondary branches (Fig. 1, A to C). Statistical analysis revealed that panicle length and both primary and secondary branch number were significantly reduced, leading to a dramatic reduction of grain number per panicle (Fig. 1, D to G). Meanwhile, several other agronomic traits were also altered in the *pal1* mutant, such as plant height, tiller number, and higher-order tillers (Supplemental Fig. S1, A to D). The flag leaf length and width as well as the internode diameter were also markedly reduced in the *pal1* mutant (Supplemental Fig. S1, E to I).

Pal1 affects IM activity

Rice aboveground organs, such as leaves, stems, and inflorescences, are all derived from the SAM. The defective phenotypes of the *pal1* mutant could be caused by a reduction of SAM activity. Thus, we first measured the size of the SAM at the 14-d-old seedling stage. Compared with WT, the SAM of the *pal1* mutant exhibited reduced size, although the structure was still normal (Fig. 2A). The longitudinal area of SAM in the *pal1* mutant was significantly reduced (by 10.5%) compared with the WT (Fig. 2B). We also observed IM at the panicle initiation stage using scanning electron microscopy (SEM), and a similar reduction was observed (Fig. 2C). Statistical analysis suggested that the basal area of the IM was markedly reduced in the *pal1* mutant (Fig. 2E). At the primary branch protruding stage, WT plants generated inflorescences with 12 to 14 primary branch meristems (PBM), whereas the PBM number in the *pal1* mutant varied from 10 to 12 (Fig. 2, D and F). These results suggest that the defective aboveground organs in the *pal1* mutant were caused by reduced meristem activity.

KNOXs are indispensable for meristem maintenance, as loss-of-function mutations of *KNOXs* result in defects in inflorescence morphology (Long et al. 1996; Tsuda et al. 2011). Therefore, we measured the transcript levels of several *KNOX* genes such as *OSH1*, *OSH3*, *OSH6*, *OSH15*, and *OSH43* in the shoot base (SB) at the tillering stage and in young panicles (~0.5 cm) using RT-qPCR. The expression levels of *OSH1* and *OSH6* were unchanged in both tissues (Fig. 3, A and B), although *OSH1* was well-characterized as a meristem marker gene (Zhang and Yuan 2014). *OSH15* was tentatively or significantly downregulated in the SB and panicle, respectively (Fig. 3, A and B). The expression level of *OSH3* was dramatically reduced in the *pal1* panicle but undetectable in the SBs of both WT and *pal1* (Fig. 3, A and B), as previously reported (Sentoku et al. 1999). mRNA in situ hybridization confirmed the downregulation of *OSH3* in the *pal1* mutant at the IM initiation stage and the PBM protruding stage (Fig. 3, C and D). Moreover, *OSH43* was upregulated in both tissues, probably resulting from a compensating response (Fig. 3, A and B). These results suggest that the *pal1* mutation could affect meristem size by regulating the expression of defined *KNOX* genes (*OSH3*, *OSH15*, *OSH43*) other than *OSH1*.

We also examined the expression of several other genes involved in meristem activity and panicle development in rice. *OsWUSCHEL* (*OsWUS*), encoding a positive regulator of IM development, was downregulated in young *pal1* panicles, whereas *FLORAL ORGAN NUMBER1* (*FON1*), an ortholog of *Arabidopsis CLAVATA1* (*CLV1*) encoding a negative regulator of IM development (Suzaki et al. 2004), was upregulated in young *pal1* panicles (Fig. 3E). The downregulation of *OsWUS* was further validated by mRNA in situ hybridization (Fig. 3F). Several other genes associated with panicle development, including *APO2/RFL*, *ASP1*, and *RCN2*, were also downregulated in the young mutant panicles (Fig. 3G). Taken together, we propose that PAL1 controls rice inflorescence architecture by affecting the expression of various genes involved in panicle development, especially meristem activity.

PAL1 encodes the CK receptor OHK4/OsHK4

An F_2 population was created by crossing the *pal1* mutant with *indica* rice cv. 'Dular', which displayed segregation of plants with normal and small panicles at a ratio of 3:1 (228:72, $\chi^2 = 0.16$, $\chi^2_{0.05,\,1} = 3.84$), indicating that the *pal1* mutant phenotype is controlled by a single recessive gene. The *PAL1* locus was initially mapped to chromosome 3 between the insertion–deletion (InDel) markers R3-17 and R3-20 (Fig. 4A). Further fine mapping narrowed down the *PAL1* locus to an 86 kb region (Fig. 4, B and C). This region comprises 10 putative open reading frames (ORFs) (Fig. 4C), encoding 7 functional proteins, 2 expressed proteins of unknown function, and 1 retrotransposon.

Sequencing detected a 6 bp deletion in ORF5 (*LOC_Os03g50860*), and no mutations were found in the other ORFs (Fig. 4D). Thus, *LOC_Os03g50860* was the most likely candidate for the mutated gene. *LOC_Os03g50860* encodes the CK receptor OHK4/OsHK4, which comprises a ligand-binding CHASE domain, a HK domain, a receiver-like domain, and a receiver domain (Supplemental Fig. S2). The

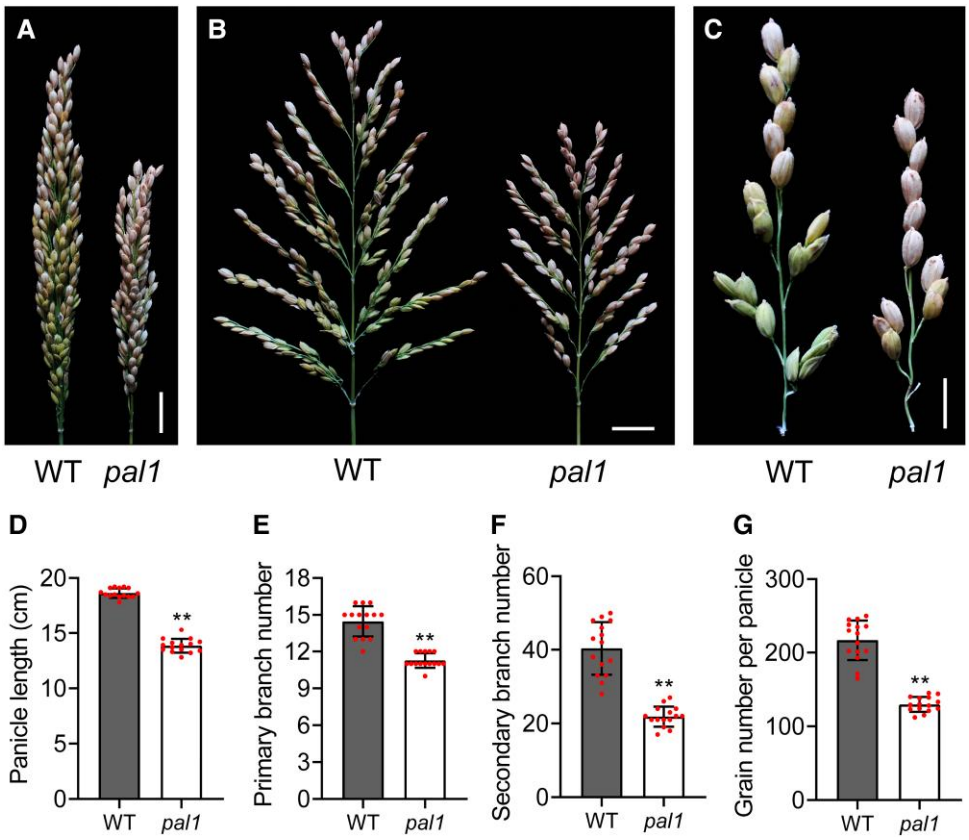

Figure 1. Morphological characterization of *pal1* panicles. **A)** and **B)** Closed **A**) and spread **B**) panicles of WT ('Huaidao 5') and *pal1* during the mature stage. Bar = 2 cm. **C)** Spread primary branches of WT and *pal1*. Bar = 0.5 cm. **D)** to **G)** Comparison of panicle length **D)**, primary branch number **E)**, secondary branch number **F)**, and grain number per panicle **G)** between WT and *pal1*. Values are given as mean ± SD ($n = 15$). $^{**}P < 0.01$ by Student's *t* test.

6 bp deletion caused the deletion of aspartic acid (D) and glutamine (Q) at the 86th and 87th residues, which are located in a highly conserved region close to the CHASE domain (Supplemental Fig. S2). The *pal1* mutant phenotype was completely rescued when WT genomic DNA of *LOC_Os03g50860* was introduced (Fig. 4, E and F). We obtained 10 rescued lines (B590) in T_0 generation, and the T_1 transgenic plants showed comparable panicle morphologies to the WT (Fig. 4, G to J). Meanwhile, we isolated 4 allelic mutants of *LOC_Os03g50860* in *japonica* rice variety 'Zhonghua 11' using Targeting Induced Local Lesions IN Genomes (TILLING) technology (Supplemental Fig. S3A) (Jiang et al. 2013), which also showed reduced panicle size (Supplemental Fig. S3, B to G). Therefore, *LOC_Os03g50860* is the causal gene of the *pa1* mutant and is referred to as *PAL1* hereafter.

Expression pattern of *PAL1* and subcellular localization of its encoded protein

To define the expression pattern of *PAL1*, we performed RT-qPCR using transcripts from various tissues. *PAL1* was highly expressed in young tissues, such as young root (R), leaf blade (LB), and leaf sheath (LS) tissues but was expressed at lower levels in these tissues at the older stage of development (Fig. 5A). *PAL1* was also highly expressed in internodes (INs) and panicles of various lengths (Fig. 5A). Histochemical staining of *ProPAL1:GUS* transgenic rice plants showed high expression of *GUS* in tissues such as young primary roots (Supplemental Fig. S4A), the sites of lateral root initiation (Supplemental Fig. S4B), and young LBs and sheaths (Supplemental Fig. S4, D and E). In the older root system, the GUS signal was mainly detected in lateral roots (Supplemental Fig. S4C). Notably, strong GUS signals were detected in stems and panicles, especially younger panicles (Supplemental Fig. S4, F and G), consistent with the results of RT-qPCR analysis. These results demonstrate that *PAL1* is mainly expressed in young tissues with active cell division.

We further examined the precise expression pattern of *PAL1* during panicle development by in situ hybridization. *PAL1* transcripts were enriched throughout the SAM and branch meristems (primary and secondary; Fig. 5, B to E) but were barely detected in spikelet meristems (SMs) (Fig. 5F). These results indicate that *PAL1* mainly functions in the early stages of panicle development.

To examine the subcellular localization of PAL1, we coexpressed PAL1-GFP fusion protein with the endoplasmic reticulum (ER) marker HDEL-mCherry (Nelson et al. 2007) in

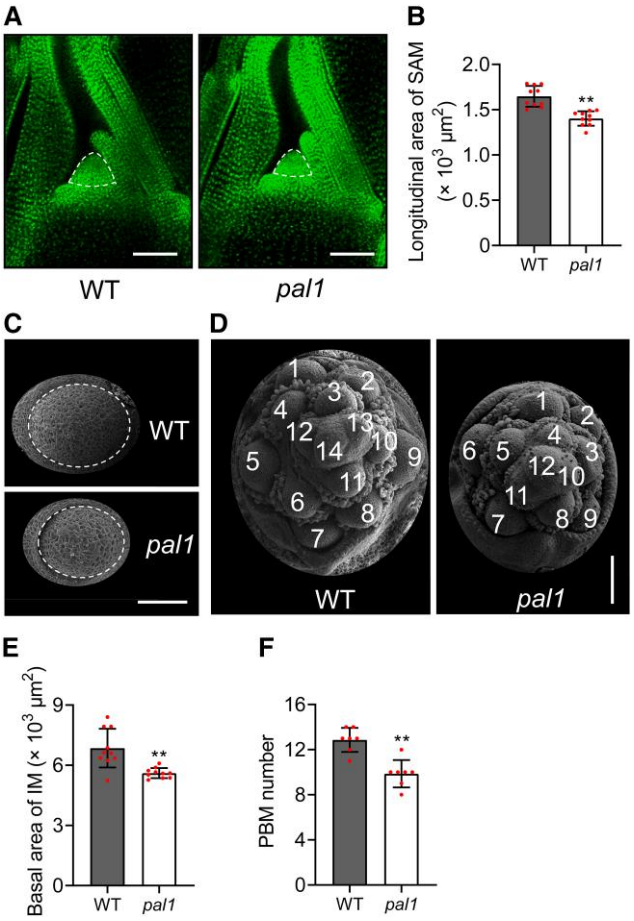

Figure 2. Comparison of SAMs and IMs between WT and *pal1* plants. **A)** SAM (surrounded by dotted lines) of WT ('Huaidao 5', left) and *pal1* (right) at the vegetative stage, stained by H33342. Samples were collected from hydroponically grown 14-d-old seedlings. Bar = 50 μm. **B)** Comparison of longitudinal area of the SAM between WT and *pal1*. **C)** Scanning electron microscopy (SEM) of IMs (surrounded by dotted lines) of WT (upper panel) and *pal1* (lower panel) undergoing the transition from the vegetative to reproductive phase. Samples in **C)** and **D)** were collected at the late tillering stage and inflorescence development stage, respectively, from rice plants grown in the paddy field. Bar = 30 μm. **D)** SEM of IM of WT (left) and *pal1* (right) at the stage of PBM formation. Bar = 100 μm. Each number represents 1 PBM. **E)** and **F)** Comparison of the IM basal area **E**) and PBM number **F**) between WT and *pal1*. Values are given as mean ± SD, $n = 10$ in **B)** and **E)**, $n = 7$ in **F)**. $^{**}P < 0.01$ by Student's t test.

leaf epidermal cells of *Nicotiana benthamiana*. The green fluorescence of PAL1-GFP was detected in a porous structure and merged with the ER marker (Fig. 5, G to J), suggesting that PAL1 is localized mainly in the ER, consistent with other CK receptors (Caesar et al. 2011; Lomin et al. 2011, 2018b; Wulfetange et al. 2011; Ding et al. 2017; reviewed in Romanov et al. 2018).

pal1 shows impaired OHK4 dimerization and OHK4 CK-binding capacity

Similar to bacterial HKs, CK receptors in plants act as homo- or heterodimers (Gao and Stock 2009; Hothorn et al. 2011; Lomin et al. 2018b). The 2-amino acid deletion of PAL1 in the *pal1* mutant is positioned close to the middle of the long α-helical stalk, which bears PAS and PAS-like subdomains (Fig. 6A). To investigate the function of the long α-helical stalk and to detect whether the *pal1* mutation affects the dimerization of the CK receptor, we performed a split-ubiquitin membrane yeast 2-hybrid assay. $PAL1^{WT}$ protein strongly interacted with itself, but $PAL1^{mu}$ failed to interact with $PAL1^{WT}$ or $PAL1^{mu}$ (Fig. 6B). These results were further verified by a split-luciferase (LUC) assay in *N. benthamiana* leaves (Fig. 6C). These data indicate the failure of receptor homodimerization in the *pal1* mutant.

To determine the effects of the mutation on the ligand-binding capacity of the receptor, we fused extracytosolic sensory modules of PAL1 from the WT or *pal1* mutant to the N-terminus of eGFP and expressed the fusion proteins in *N. benthamiana* leaves (Supplemental Fig. S5, A and B). We isolated leaf microsomes and used them for a binding assay with the radiolabeled CK [^{3}H]isopentenyladenine (^{3}H-iP) (Lomin et al. 2015, 2018a). We measured total and nonspecific binding of [^{3}H]iP (Supplemental Fig. S5C) and normalized these values to the quantity of OHK4 in the probe, as detected by examining the fluorescence of the fused eGFP. The calculated specific binding of the *pal1* mutant protein was dramatically reduced (by ~4.7-fold) compared with WT PAL1 binding (Fig. 6D). These results indicate that the D86-Q87 deletion in the long α-helical stalk of the sensor module has a substantial effect on the CK-binding capacity of the receptor.

PAL1 is required for CK signaling and responses to exogenous CKs

Exogenously supplying CKs can inhibit root growth, while the deficiency of CK signaling alleviates this inhibition (Ueguchi et al. 2001; Ding et al. 2017). Thus, we treated WT and *pal1* seedlings with *trans*-zeatin (tZ). In the WT, root growth was severely inhibited with increasing tZ concentration. However, this inhibition was weaker in the *pal1* mutant (Fig. 7, A and B), indicating that *PAL1* takes part in exogenous CK sensing in roots.

Applying CKs can also inhibit leaf senescence (Hutchison et al. 2006; Sun et al. 2014). Under dark treatment, both WT and *pal1* leaves progressively turned yellow due to the loss of chlorophyll. Applying tZ delayed leaf senescence in WT, while leaf senescence was barely affected by tZ in the *pal1* mutant (Fig. 7C). Measurement of chlorophyll content on the 7th day of treatment revealed that the stability of chlorophyll gradually increased with increasing tZ concentration in the WT but remained consistently low in the *pal1* mutant (Fig. 7D).

Type-A RR genes (type-A *RRs*) are inducible by CK and considered to be primary CK response genes (Taniguchi et al. 1998; D'Agostino et al. 2000). RT-qPCR analysis revealed that the expression of most type-A *RRs* was reduced in the SB of the *pal1* mutant (Supplemental Fig. S6A), whereas only a few of these genes were downregulated in the panicle

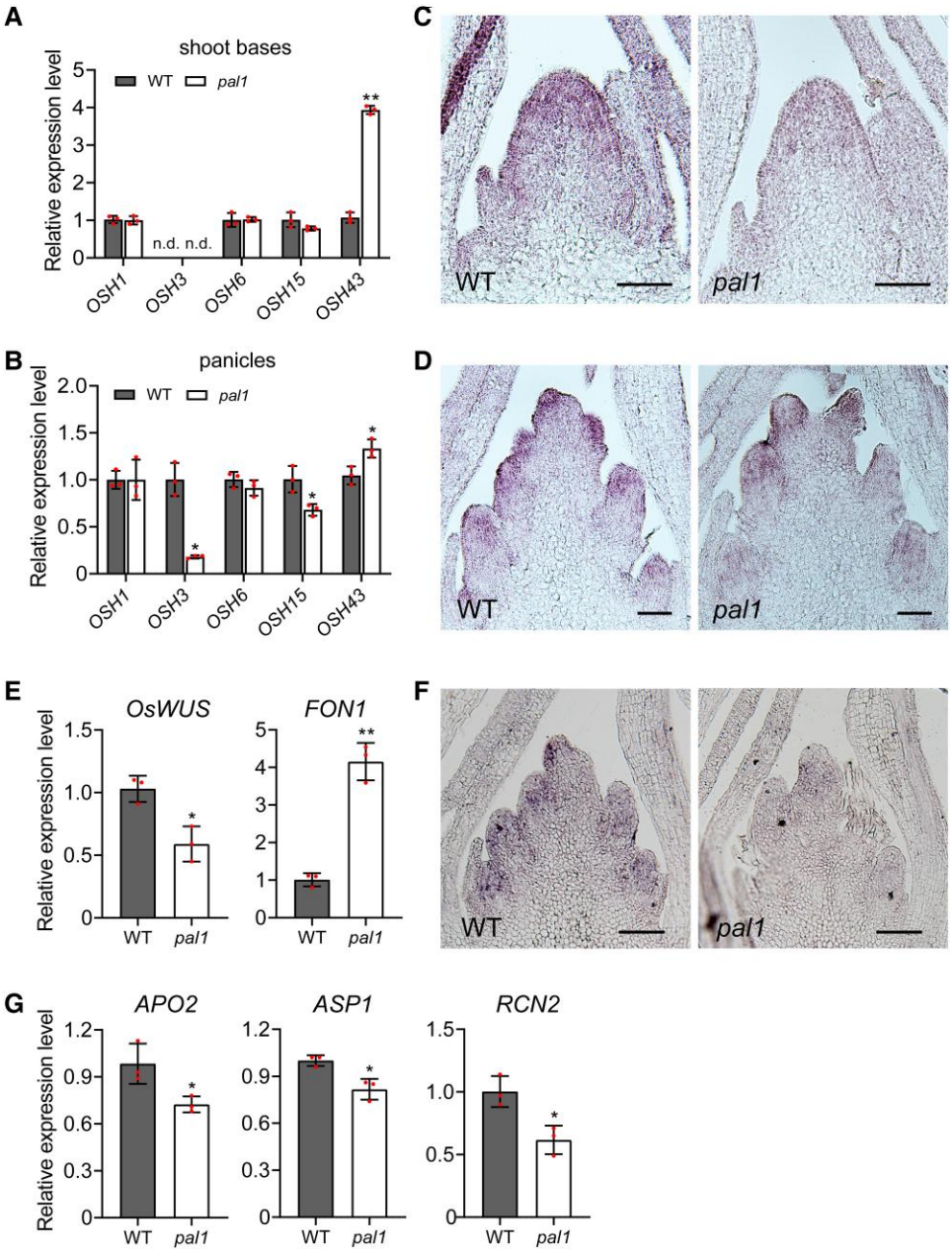

Figure 3. Expression of genes involved in meristem activity and panicle development in WT and *pal1* plants. **A)** Comparison of *OSH* expression in the SB at the tillering stage from plants grown in the paddy field by RT-qPCR between WT ('Huaidao 5') and *pal1*. n.d., not detected. **B)** Comparison of *OSH* expression in young panicles (~0.5 cm) by RT-qPCR between WT and *pal1*. **C)** Comparison of *OSH3* mRNA levels in the IM transition phase by in situ hybridization between WT (left) and *pal1* (right). Bar = 50 μm. **D)** Comparison of *OSH3* mRNA levels in the PBM initiation phase by in situ hybridization between WT (left) and *pal1* (right). Bar = 50 μm. **E)** Comparison of *OsWUS* and *FON1* expression in young panicles by RT-qPCR between WT and *pal1*. **F)** Comparison of *OsWUS* mRNA levels in the PBM initiation phase by in situ hybridization between WT (left) and *pal1* (right). Bar = 50 μm. **G)** Comparison of *APO2*, *ASP1*, and *RCN2* expression in young panicles by RT-qPCR between WT and *pal1*. Values are given as mean ± SD ($n = 3$). *$P < 0.05$ and **$P < 0.01$ by Student's t test.

(Supplemental Fig. S6B). Among these, *OsRR1*, a marker gene of CK signaling in the SAM and IM (Jain et al. 2006; Li et al. 2013), was downregulated in both tissues. We then compared the dynamic response of *OsRR1* transcript with tZ treatment in SBs. In the WT, *OsRR1* expression was rapidly induced at 0.5 h after tZ application and reached the peak by 1 h, followed by a drop. However, only a very low level of induction was detected in the *pal1* mutant (Fig. 7E). mRNA in situ hybridization further confirmed the marked reduction of *OsRR1* expression in the IM of the *pal1* mutant (Fig. 7F). These results indicate that CK signal transduction was strongly suppressed in the *pal1* mutant. We also examined the expression levels of several type-B *RRs* (*OsRR21-OsRR26*) in the young panicle. *OsRR21* and *OsRR26*

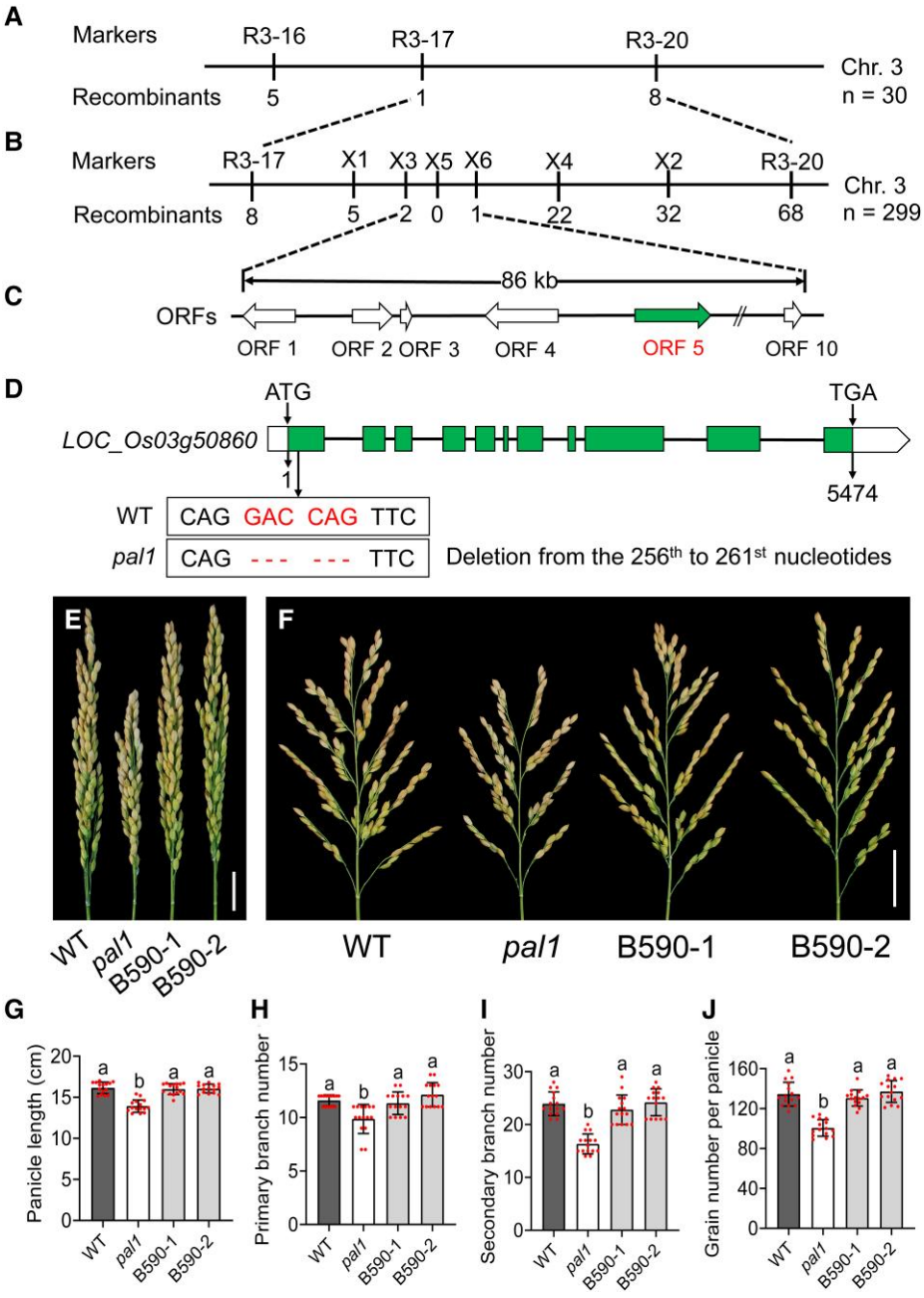

Figure 4. Map-based cloning of *PAL1* and genetic complementation. **A)** The *PAL1* locus was mapped to a region between InDel markers R3-17 and R3-12 on chromosome 3. **B)** and **C)** Fine mapping of *PAL1*. The *PAL1* locus was further delimited to an 86 kb genomic region between markers X3 and X6, which contains 10 ORFs. The number of recombinants is indicated beneath the marker positions. **D)** Schematic structure of the *PAL1* gene. The boxes and lines represent exons and introns, respectively. The start codon (ATG) and the stop codon (TGA) are indicated. A 6 bp deletion from the 256th to 261st nucleotide in *PAL1* resulted in the dropping-out of aspartate (D) and glutamine (Q) residues. **E)** and **F)** Complementation assay. Panicles of 2 genomic DNA complementation transgenic lines (B590) are shown. Bar = 2 cm. **G)** to **J)** Statistical comparison of panicle length **G)**, primary branch number **H)**, secondary branch number **I)**, and grain number **J)** among the WT ('Huaidao 5'), *pal1*, and the complemented lines. Values are given as mean ± SD ($n = 15$). The different letters above the histogram indicate significant differences ($P < 0.05$) by 1-way ANOVA followed by Turkey's multiple comparison test.

expression showed a slight increase in the *pal1* panicle vs. the WT, while the others remained unchanged (Supplemental Fig. S6C).

Two-component signaling sensor new (TCSn) is a synthetic CK-sensitive promoter (Müller and Sheen 2008; Zürcher et al. 2013). To further assess the CK signaling status of the *pal1* mutant, the *ProTCSn:GUS* construct was transformed into +/*pal1* heterozygotes, and the homozygous progenies were subjected to GUS staining. Compared with WT, the GUS signal was much weaker

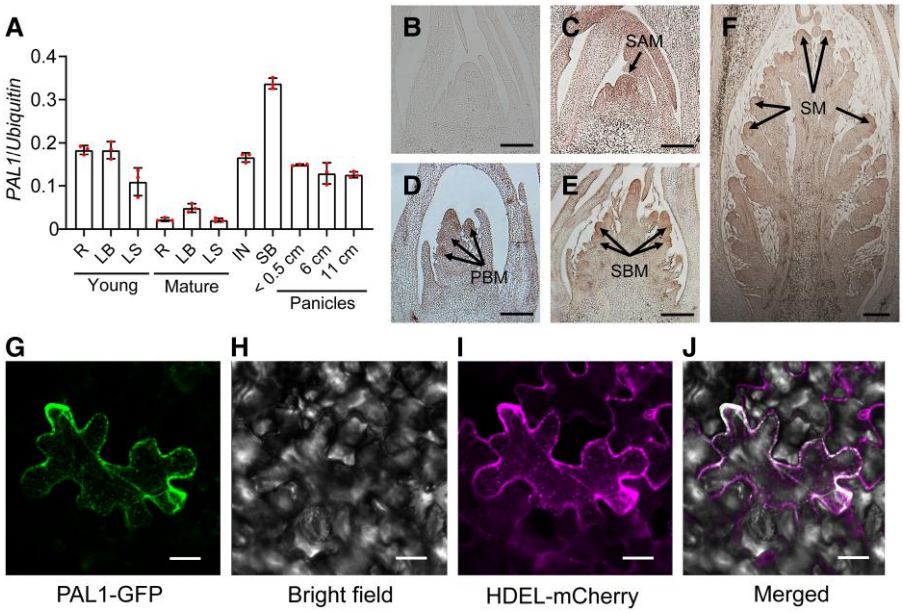

Figure 5. Expression pattern of *PAL1* and subcellular localization of its encoded protein. **A)** *PAL1* expression levels revealed by RT-qPCR in various organs. The rice *Ubiquitin* gene was used as an internal control. The young R, LB, and LS were collected from hydroponic seedlings at 3 wks, while the mature R, LB, LS, and IN were collected from 12-wk-old plants grown in the paddy field. The SB was collected from 9-wk-old plants grown in the paddy field. Values are given as mean ± SD ($n = 3$). **B)** to **F)** *PAL1* mRNA levels at various stages of panicle meristem development revealed by in situ hybridization. **B)** Hybridization using a sense probe as a negative control. **C)** SAM at the transition stage from the vegetative to reproductive phase. **D)** PBM initiation stage. **E)** SBM formation stage. **F)** SM formation stage. Bar = 100 μm in **B)** to **E)**. Bar = 200 μm in **F)**. **G)** to **J)** Subcellular localization of PAL1 protein. PAL1-GFP **G)** and the ER marker mCherry-HDEL **I)** were coexpressed in *N. benthamiana* leaves. **H)** Bright field. **J)** Merged image of PAL1-GFP and HDEL-mCherry. More than 10 independent cells were observed, which showed a consistently merged signal in the ER. Bar = 20 μm.

in both roots and young panicles of the *pal1* mutant (Fig. 7G), indicating that *PAL1* is required for the output of CK signaling.

The *pal1* mutation disturbs endogenous CK homeostasis

Previous studies suggested a metabolic link between CK signaling and homeostasis in *Arabidopsis* (Riefler et al. 2006; Bartrina et al. 2017). To test such a link in rice, we measured the endogenous CK contents in young panicles (~0.5 cm). Compared with WT, the concentrations of tZ, iP, and their ribosides and glucosides were significantly reduced in the *pal1* mutant (Fig. 8A).

To examine the possible reasons for the reduced steady-state CK concentration in the *pal1* mutant, we measured the expression levels of genes involved in CK biosynthesis and degradation. *OsIPTs* and *LOGs*, encoding isopentenyl transferases and CK-activating enzymes (Sakamoto et al. 2006; Kurakawa et al. 2007), respectively, were all upregulated to various extents in the *pal1* mutant vs. the WT (Fig. 8, B and C). *OsCKXs* which encode CK oxidases/dehydrogenases involved in CK degradation (Ashikari et al. 2005) were also upregulated in the mutant (Fig. 8, D to G). Notably, *OsCKX2* expression strongly increased in the young panicles of *pal1* (Fig. 8D). mRNA in situ hybridization also revealed strongly increased expression of *OsCKX2* in the IM at the initiation stage and in primary and secondary branch meristems (SBMs) (Fig. 8H).

Taken together, the *pal1* mutation affects CK homeostasis through the upregulation of genes involved in both CK biosynthesis and degradation. The drastic rise in *OsCKXs* expression, especially (but not only) *OsCKX2*, could be the major reason for the reduced endogenous CK levels in the *pal1* mutant, which may in turn contribute to the reduction of meristem activity and the underdevelopment of inflorescences.

IPA1 is upregulated by the PAL1-OsRR21 cascade

To identify the possible downstream effectors, we examined the expression of several genes related to meristem and panicle development in rice (Fig. 3). Among these genes, *OsWUS* and *OSH1* were reported to be involved in CK signaling. However, *OsWUS* primarily controls rice tiller number rather than panicle length (Lu et al. 2015; Tanaka et al. 2015), while the expression of *OSH1*, which positively responds to CK signaling (Naruse et al. 2018), was not altered in the *pal1* mutant. Both *OSH15* and *IPA1* (also known as *OsSPL14*/*WFP*) were downregulated to various degrees in the SBs and young panicles (Figs. 3, A and B, and 9A). Previous studies have shown that OSH15 is associated with CK, as it recruits PRC2 to the *OsCKX4* promoter and represses its transcription, ultimately controlling rice panicle architecture (Wang et al. 2022). However, the relationship between CK and

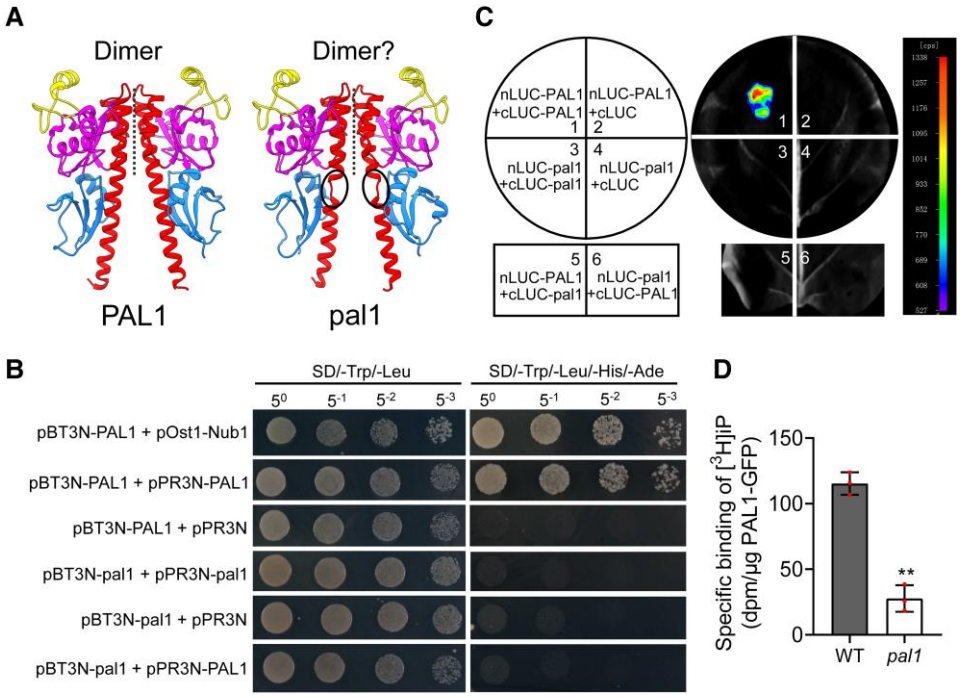

Figure 6. Homodimerization and ligand-binding capacity of WT and mutant PAL1 protein. **A)** Three-dimensional models of homodimers of the PAL1 (OHK4) extracellular domain of WT (left) and the mutant (right). Modeling was accomplished in Modeller software (Šali and Blundell 1993). Stereochemical quality of the models was assessed with ProCheck (Laskowski et al. 1993) implemented in PDBsum Web service (Laskowski et al. 2018). Visualization of the models was accomplished with UCSF Chimera (Pettersen et al. 2004). Dotted lines indicate dimerization interfaces. The deletion in *pal1* is indicated by circles. **B)** Homodimerization of PAL1 protein revealed by the split-ubiquitin membrane yeast 2-hybrid assay. The prey pOst1-Nub1 (which expresses a fusion of the yeast ER-resident protein Ost1 to the Nub portion of yeast ubiquitin) and empty pPR3N vector were used as positive and negative controls, respectively. **C)** Homodimerization of PAL1 protein revealed by split-LUC complementation assay in *N. benthamiana* leaves. **D)** Comparison of the ligand-specific binding capacity of PAL1 (OHK4) protein between WT and *pal1*. [^{3}H] iP-PAL1 binding was measured in a plant (*N. benthamiana* microsomes) assay system. Three independent binding assays were conducted for the WT and *pal1* protein, respectively. Values are given as mean ± SD ($n = 3$). $^{**}P < 0.01$ by Student's t test.

IPA1 remains unclear. Another study in Arabidopsis showed that control of the vegetative phase change by CK relies on the function of SPL transcription factors (Werner et al. 2021), which prompted us to explore the relationship between *PAL1* and *IPA1*. Therefore, we performed an mRNA in situ hybridization assay, which validated the decreased expression of *IPA1* at the IM and PBM initiation stages (Fig. 9B). To investigate whether CK has an immediate impact on the expression of *IPA1*, we examined the time course of *IPA1* expression in tZ-treated SBs of hydroponically grown 10-d-old seedlings. In WT, *IPA1* expression was induced after 30 min of treatment, reached a peak at 1 h, and then decreased. However, *IPA1* was only slightly induced by tZ treatment in the *pal1* mutant, and no obvious expression peak was detected (Fig. 9C). Therefore, *IPA1* may act downstream of the CK signaling mediated by *PAL1*.

To validate this hypothesis, we first searched for CK response elements (5′-(A, G)GAT(C, T)-3′ or 5′-AAGAT(C, T)TT-3′) (Hosoda et al. 2002; Zubo et al. 2017) in the promoter of *IPA1*. Ten such elements were identified within the 2 kb region upstream of the start codon (Fig. 9D), suggesting that *IPA1* could be regulated by type-B RRs. *OsRR21*, *OsRR22*, and *OsRR23* contribute to rice panicle architecture, while loss-of-function of *OsRR24* has no effect on inflorescence size (Worthen et al. 2019; Yamburenko et al. 2020). To evaluate the regulatory relationship between *IPA1* and type-B OsRRs, we performed transient transcriptional assays using the dual-LUC system in *N. benthamiana* leaves (Fig. 9E). OsRR21 and OsRR22 greatly facilitated the expression of *LUC* driven by the *IPA1* promoter, but OsRR23 had no significant effect (Fig. 9F). Notably, the transcriptional activation of *IPA1* conferred by OsRR21 was higher than that by OsRR22.

To test whether OsRRs could directly bind to the *IPA1* promoter, we performed yeast 1-hybrid (Y1H) assays. OsRR21 bound to probes P1, P2, P3, and P8 containing the first, second, third, and ninth CK response element, respectively (Fig. 9G). In contrast, OsRR22 only bound to P5, and OsRR23 bound to none of these probes (Supplemental Fig. S7). We also found that the P5 probe could be bound by OsRR26, whose transcripts displayed the same upregulation as *OsRR21* in the *pal1* mutant (Supplemental Fig. S7). These results demonstrate that OsRR21 is likely the major type-B RR that regulates *IPA1* expression. Thus, we focused on *OsRR21* for further study.

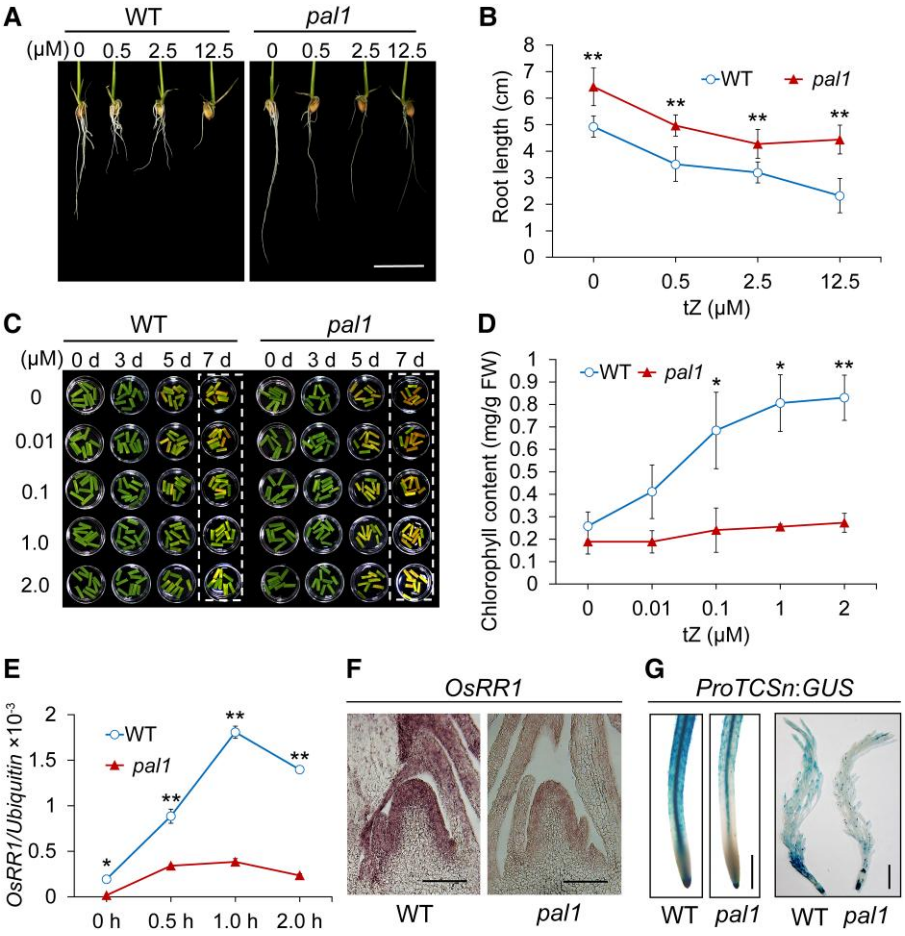

Figure 7. Reduction of CK signaling in the *pal1* mutant. **A)** Inhibition of root growth by exogenous tZ. Seedlings were treated for 10 d with various concentrations of tZ as indicated. Bar = 2 cm. **B)** Comparison of root length between WT ('Huaidao 5') and *pal1* plants on the 10th day of treatment. **C)** Exogenous tZ delayed dark-induced leaf senescence. Leaves were treated with various concentrations of tZ as indicated for 3, 5, and 7 d. **D)** Comparison of chlorophyll content between WT and *pal1* on the 7th day of tZ treatment (samples in the boxed region of **C)**). **E)** Comparison of time-course expression of *OsRR1* induced by 1 μM tZ in the SB of hydroponically grown 10-d-old seedlings between WT and *pal1*. **F)** Comparison of the *OsRR1* mRNA levels between WT and *pal1* by in situ hybridization. The IMs were sampled just after the transition from the vegetative to reproductive phase. Bar = 100 μm. **G)** GUS staining of the root (left) and panicle (right) of the CK-responsive *ProTCSn:GUS* reporter in WT and *pal1* plants. Bars are 0.5 mm (left) and 1 cm (right). Values are given as mean ± SD. $n = 10$ in **B)**, $n = 3$ in **D)** and **E)**. $^*P < 0.05$ and $^{**}P < 0.01$ by Student's t test.

We overexpressed OsRR21 with a HA-tag fused to the N-terminus driven by the maize *Ubiquitin* promoter in WT ('Huaidao 5'). A total of 23 T_0 lines were obtained. The T_1 *HA-OsRR21* overexpression plants displayed significantly increased primary branch number, whereas they were comparable with WT in terms of plant height, tiller number, panicle length, secondary branch number, and grain number (Supplemental Fig. S8, F to I). Overexpression of *OsRR21* in these plants was confirmed by RT-qPCR (Fig. 9I). We then performed a chromatin immunoprecipitation (ChIP)-qPCR assay using *HA-OsRR21* transgenic seedlings. Consistent with the Y1H results, the specific regions containing P1, P2, P3, and P8 were markedly enriched (Fig. 9H). Additionally, we measured *IPA1* transcript levels in panicles of the *HA-OsRR21* overexpression lines. *IPA1* was upregulated in these panicles, and its expression levels were positively correlated with those of *OsRR21* (Fig. 9, I and J). These results suggest that *IPA1* is regulated by CK signaling mediated by the PAL1-OsRR21 cascade.

OsRR21 protein contains a Myb-like GARP DNA-binding domain in the central region and a RR domain at the N-terminus that perceives CK signaling through a His-to-Asp phosphorelay (Fig. 9K) (Heyl and Schmülling 2003; Kakimoto 2003). To investigate whether OsRR21 functions downstream of PAL1, we compared the in vivo phosphorylation levels of OsRR21 in WT and *pal1* protoplasts. Since the full-length OsRR21 protein was barely expressed in rice protoplasts, we expressed a truncated OsRR21 (1 to 188 aa) protein named RR21N that contains the RR domain and a myc-tag the N-terminus (Fig. 9K). When separated on the phos-tag gel, a weak shifted band was detected compared with those separated on a normal

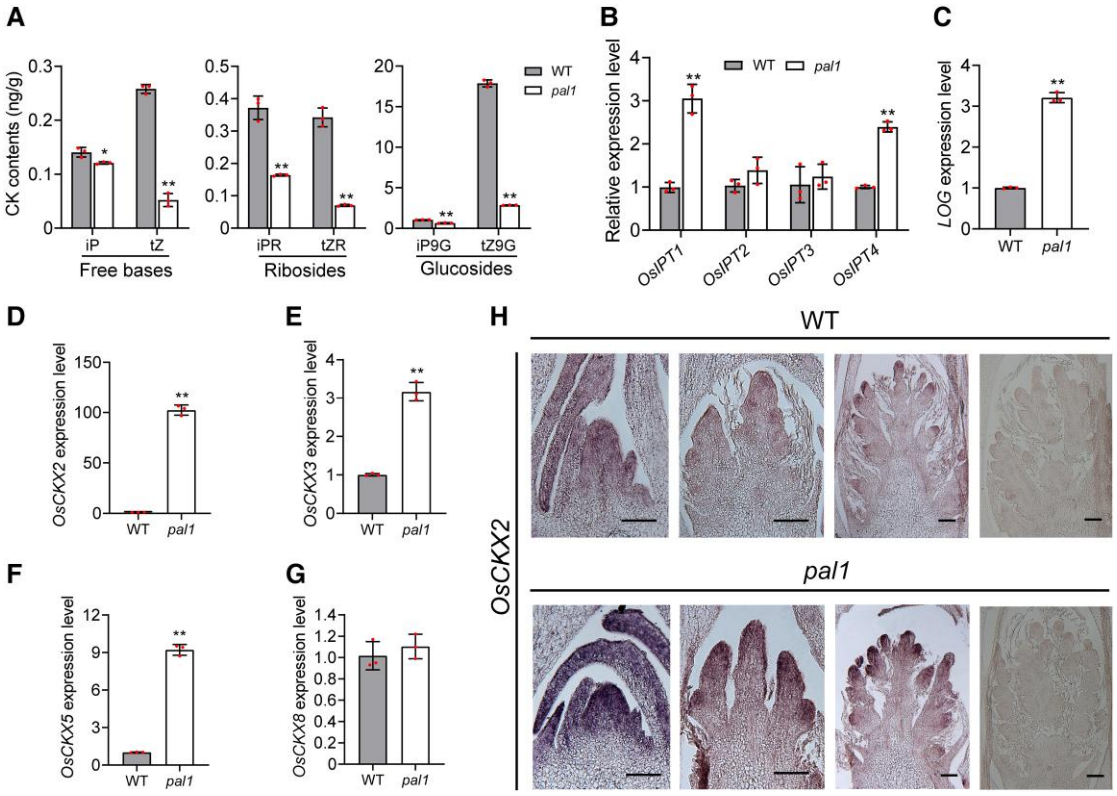

Figure 8. The *pal1* mutation affects endogenous CK homeostasis. **A)** Comparison of CK contents in young panicles (~0.5 cm) between WT ('Huaidao 5') and *pal1*. **B)** and **C)** Comparison of the expression of CK biosynthesis genes *OsIPTs* and *LOG* between WT and *pal1*. Samples are panicle ~0.5 cm in length (the same below). **D)** to **G)** Comparison of the expression of *OsCKX2* **D)**, *OsCKX3* **E)**, *OsCKX5* **F)**, and *OsCKX8* **G)** between WT and *pal1*. **H)** Comparison of *OsCKX2* mRNA levels at various stages of IM development revealed by in situ hybridization. The stages of meristems are as mentioned in Fig. 5. Photographs on the far right are negative controls hybridized with sense probes. Bar = 100 μm. Values are given as mean ± SD ($n = 3$). *$P < 0.05$ and **$P < 0.01$ by Student's t test.

PAGE gel (Supplemental Fig. S9). The application of calf intestine alkaline phosphatase (CIP) eliminated the weak shifted band, confirming that the shifted band was the phosphorylated form of RR21N (RR21N-P) (Fig. 9K). RR21N-P was present in both WT and the *pal1* mutant at similar levels (Fig. 9L). However, when the CK 6-BA was applied, the shifted bands in the WT (3 replicates) became more pronounced than those in the *pal1* mutant (Fig. 9L), suggesting that the response of OsRR21 to CK signaling is weaker in the *pal1* mutant and that its RR phosphorylation is PAL1-dependent.

To further analyze the genetic relationship between *PAL1* and *OsRR21*, we overexpressed *OsRR21* in the *pal1* mutant. A total of 10 T_0 lines were obtained. Compared with the *pal1* mutant and its original WT ('Huaidao 5'), the T_1 *OsRR21* overexpression lines (Fig. 10K) could not rescue the plant height and tiller number phenotype of the *pal1* mutant (Fig. 10, A, E, and F). Higher-order tillers bearing smaller panicles were still present in the *OsRR21* overexpression lines (Fig. 10B). However, the phenotype of panicles generated on primary tillers was largely rescued in the *OsRR21* overexpression lines. Panicle length and secondary branch number were recovered to the WT level (Fig. 10, C, D, G, and I), while the primary branch number became even higher than the WT (Fig. 10H), perhaps leading to slightly more grains than the WT, although this increase was not significant (Fig. 10J). These observations suggest that overexpressing *OsRR21* at least partially recovered the *pal1* mutant phenotype.

Collectively, these data indicate that *OsRR21* is a direct target of PAL1-mediated CK signaling in controlling rice inflorescence architecture. *IPA1* acts downstream of CK signaling, and its expression is affected by the PAL1-OsRR21 phosphorelay cascade.

IPA1 positively regulates *PAL1*, forming a feedback circuit

A previous ChIP sequencing (ChIP-seq) assay demonstrated that IPA1 directly binds to the promoter of *LOG* (Lu et al. 2013), suggesting a potential link between *IPA1* and CK signaling. This prompted us to reexamine the IPA1 binding profile in the promoter of *PAL1* (Lu et al. 2013). One IPA1 binding peak was identified, which encompassed 2 indirect IPA1 binding motifs (TGGGCC, P1 and P2) located 636 and 300 bp upstream of the *PAL1* start codon, respectively (Fig. 11A). To confirm the ChIP-seq result, we transformed

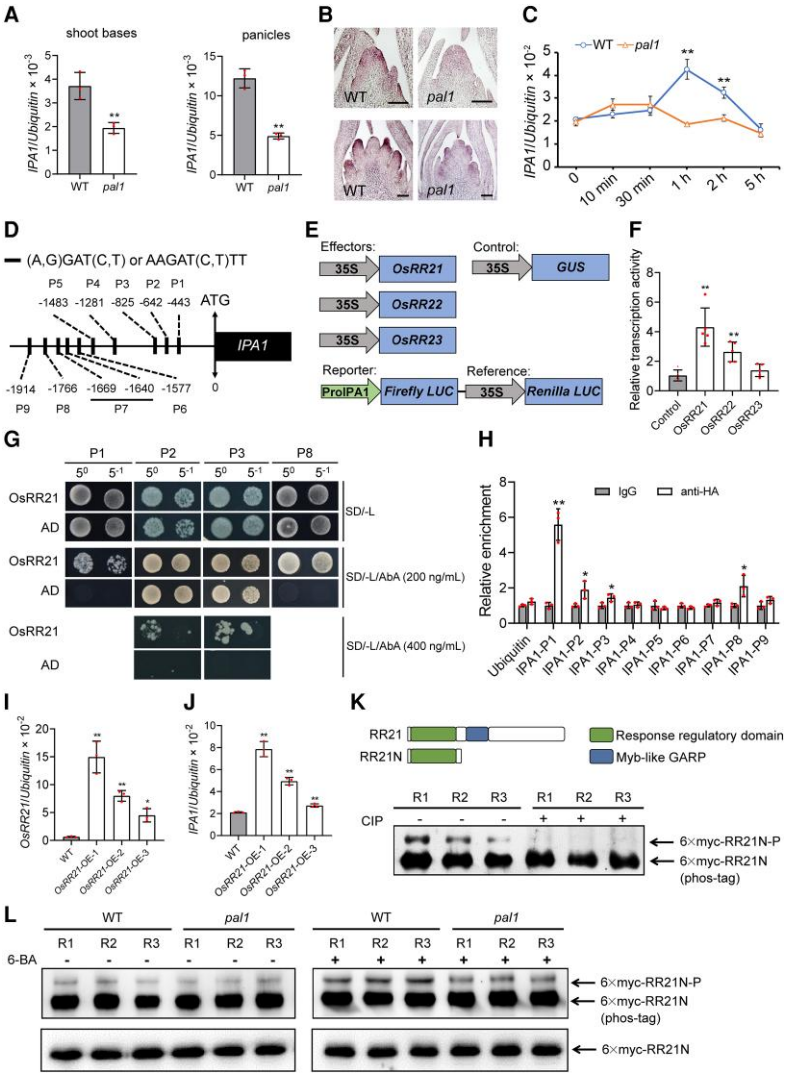

Figure 9. IPA1 functions downstream of the PAL1-OsRR21 phosphorylation pathway. **A)** Comparison of *IPA1* expression levels between WT ('Huaidao 5') and *pal1* in the SB at the tillering stage in rice plants grown in the paddy field and young panicles (~0.5 cm) by RT-qPCR. **B)** Comparison of mRNA levels of *IPA1* between WT (left) and *pal1* (right) by in situ hybridization. The upper 2 photographs correspond to the transition from the vegetative to reproductive phase. The lower 2 photographs correspond to the stage of PBM formation. Bar = 100 μm. **C)** Time-course expression of *IPA1* in the SB of hydroponically grown 10-d-old seedlings treated with 5 μM tZ. **D)** Structure of the *IPA1* promoter region. The positions of CK response elements ((A, G)GAT(C, T) and AAGAT(C, T)TT) are highlighted. Numbers indicate the distance away from the start codon ATG. "*P*" indicates the probes used for Y1H and ChIP-qPCR assays. Due to the close proximity, the 7th and 8th CK response elements were synthesized into a single probe. **E)** and **F)** Transcriptional activities of type-B OsRRs on the *IPA1* promoter in *N. benthamiana* leaves. **E)** Constructs used in **F)**. Relative transcriptional activity was calculated by LUC/REN and normalized to that of the control. A total of 5 independent infiltration assays were measured. **G)** Y1H assays showing that OsRR21 strongly binds to the probes P1, P2, P3, and P8 in the *IPA1* promoter. Empty AD (pGADT7) vector was used as a negative control. The concentrations of AbA used to screen protein–DNA interactions are indicated. **H)** ChIP-qPCR assay showing that OsRR21 binds to the promoter of *IPA1* in vivo. Chromatin isolated from *ProUBI:HA-OsRR21* transgenic seedlings was immunoprecipitated with anti-HA antibody and IgG serum, respectively. The relative enrichment was calculated by dividing the enrichment value of ChIP with anti-HA by that of ChIP with IgG serum. An upstream region of *Ubiquitin* without a CK response element was used as a negative control. **I)** and **J)** Expression levels of *OsRR21* **I)** and *IPA1* **J)** in the young panicles (~0.5 cm) of the *OsRR21* overexpression plants (WT, 'Huaidao 5'). **K)** Schematic diagram and phosphorylation of OsRR21 protein. The longer and shorter dark boxes indicate regulatory response and Myb-like GARP domains, respectively. Truncated OsRR21 (RR21N) (1 to 188 aa) was transiently expressed in rice protoplasts and detected with an anti-myc antibody for the in vivo phosphorylation assays. CIP treatment indicated that the upper shifted bands in the phos-tag gel were phosphorylated RR21N proteins. Three biological replicates (separate experiments) are displayed. **L)** The response of OsRR21 phosphorylation to CK was diminished in the *pal1* mutant. Protoplasts of WT and the *pal1* mutant transfected with RR21N were incubated for 15 h, followed by incubation with (+) or without (−) 6-BA for one more hour. Phos-tag gel was used for mobility shift, and routine SDS–PAGE indicates the equal loading of total RR21N. Three biological replicates (separate experiments) are displayed. Data are presented as mean ± SD. $n = 3$ in **A)**, **C)**, **H)**, **I)**, and **J)**. $n = 5$ in **F)**. $^{*}P < 0.05$ and $^{**}P < 0.01$ by Student's t test.

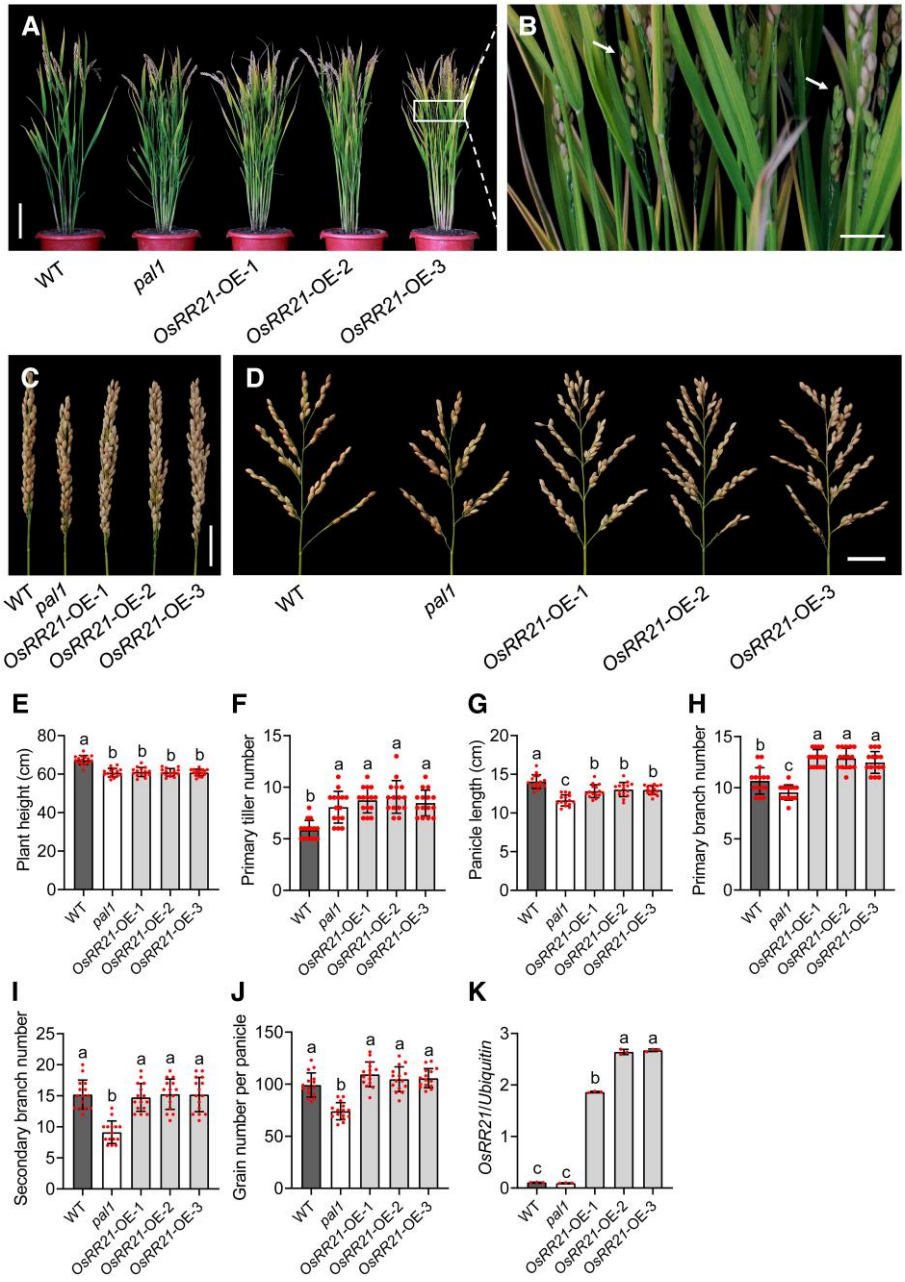

Figure 10. Overexpression of *ORR21* partially rescued the *pal1* panicle phenotype. **A)** and **B)** Plant architecture of WT ('Huaidao 5'), *pal1*, and 3 *OsRR21* overexpression lines in the *pal1* background. The higher-order tillers bearing small panicles are indicated by arrows **B)**. Bar = 20 cm in **A)**, 2 cm in **B)**. **C)** and **D)** Morphologies of closed **C)** and spread **D)** panicles generated on the primary tillers of WT, *pal1*, and *OsRR21* overexpression lines. Bar = 4 cm. **E)** to **J)** Comparison of plant height **E)**, primary tiller number **F)**, panicle length **G)**, primary branch number **H)**, secondary branch number **I)**, and grain number per panicle **J)** among WT, *pal1*, and *OsRR21* overexpression lines. Panicles in **G)** to **J)** only include those generated on primary tillers. **K)** Expression levels of *OsRR21* in the *OsRR21* overexpression plants (*pal1* background). Values are given as mean ± SD. $n = 15$ in **E)** to **J)**, $n = 3$ in **K)**. The different letters above the histogram indicate significant differences ($P < 0.05$) by 1-way ANOVA followed by Turkey's multiple comparison test.

japonica rice cultivar 'Chunjiang 06' with the *ProIPA1:7mIPA1-GFP* fusion construct according to a previous report (Jiao et al. 2010) and performed ChIP-qPCR analysis. A total of 17 lines were obtained in the T_0 generation. We analyzed transgenic lines with higher *IPA1* expression (Supplemental Fig. 10J) in the T_1 generation. As expected, the transgenic plants displayed increased plant height and reduced tiller number compared with WT ('Chunjiang 06') (Supplemental Fig. 10, A, D, and E). The panicle length, branch number, and grain number all increased in the transgenic plants vs. the WT (Supplemental Fig. 10, B, C, and F to I). ChIP-qPCR showed that the 2 specific regions

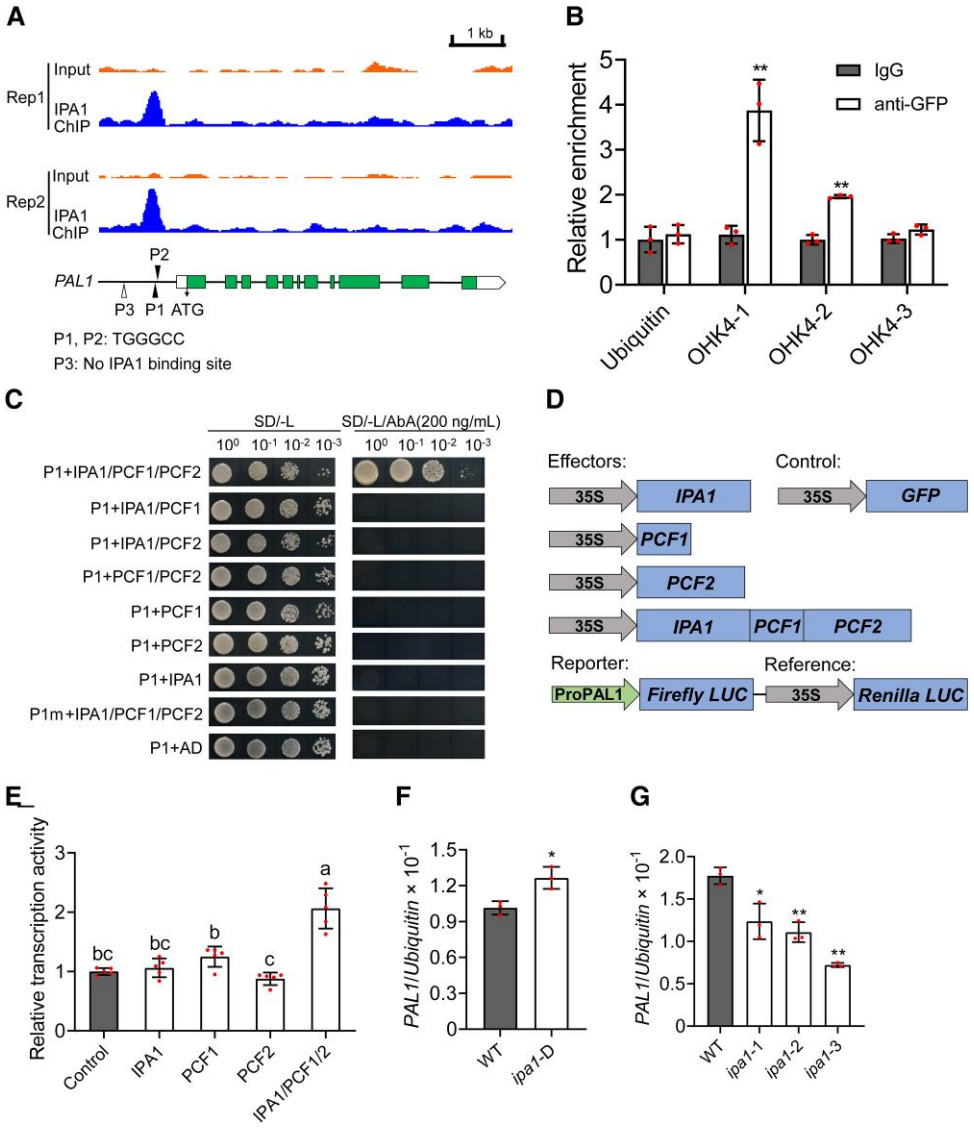

Figure 11. *PAL1* is positively regulated by IPA1. **A)** Two replicates of the IPA1 binding profile in the promoter of *PAL1*, as revealed by a previous ChIP-seq study (Lu et al. 2013). Sequencing profile of the input DNA without ChIP is shown as the background control. P1 and P2 refer to the indirect binding motif TGGGCC of IPA1. P3 is a region that does not contain an IPA1 binding site and is located outside of the IPA1 binding peak. **B)** ChIP-qPCR analysis showing that IPA1 binds to the promoter of *PAL1* in vivo. Chromatin isolated from *ProIPA1:7mIPA1-GFP* seedlings was immunoprecipitated with the anti-GFP antibody and IgG serum, respectively. The relative enrichment was calculated by dividing the enrichment value of ChIP with anti-GFP by that of ChIP with IgG serum. P3 (which lacks an IPA1 binding site) and an upstream region of *Ubiquitin* were used as negative controls. **C)** IPA1 binds to the P1 probe (containing the TGGGCC motif) of the *PAL1* promoter through interactions with PCF1 and PCF2, as revealed by a Y1H assay. P1m indicates the fragment containing a mutated motif of AGGGCC. Empty AD (pGADT7) vector was used as a negative control. AbA at a concentration of 200 ng/mL was used for selection of protein–DNA interactions. **D)** and **E)** IPA1 activates the expression of *PAL1* together with PCF1 and PCF2 in rice protoplasts. **D)** Constructs used in **E)**. Relative transcriptional activity was calculated by LUC/REN and normalized to that of the control. A total of 5 independent transient transformation assays were measured. **F)** and **G)** *PAL1* expression in young panicles (~0.5 cm long) of the gain-of-function *ipa1-D* mutant (WT, 'Huaidao 5') and the loss-of-function *ipa1* mutant (WT, 'Chunjiang 06') by RT-qPCR. Values are given as mean ± SD. $n = 3$ in **B)**, **F)**, and **G)**. $n = 5$ in **E)**. *$P < 0.05$ and **$P < 0.01$ by Student's t test. Different letters above the histogram indicate significant differences ($P < 0.05$) by 1-way ANOVA followed by Turkey's multiple comparison test.

containing P1 and P2 were significantly enriched, while no enrichment was detected for the negative control region P3 or the *Ubiquitin* promoter (Fig. 11B).

We then performed Y1H assay to further validate the binding of IPA1 to the TGGGCC motif in the *PAL1* promoter. Since IPA1 targets the TGGGCC motif through interactions with 2 TCP family members, PCF1 and PCF2 (Lu et al. 2013), different combinations of IPA1, PCF1, and PCF2 were tested. Immunoblotting showed that all prey proteins (GAL4 AD-IPA1, GAL4 AD-PCF1, and GAL4 AD-PCF2) were properly expressed in yeast cells (Supplemental Fig. 11). IPA1 bound to a 66 bp probe containing the P1 motif only

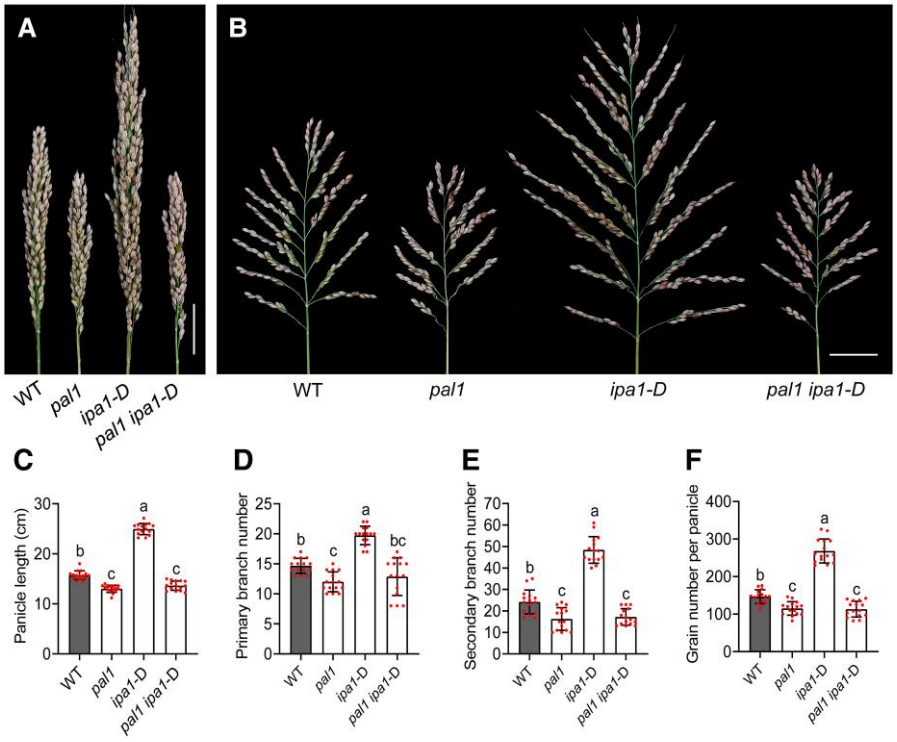

Figure 12. *IPA1* acts upstream of *PAL1* to regulate rice inflorescence architecture. **A)** and **B)** Closed **A)** and spread **B)** panicle morphologies of WT ('Huaidao 5'), *pal1*, *ipa1-D*, and *pal1 ipa1-D* double mutant. Bar = 4 cm. **C)** to **F)** Comparison of panicle length **C)**, primary branch number **D)**, secondary branch number **E)**, and grain number per panicle **F)** among WT, *pal1*, *ipa1-D*, and *pal1 ipa1-D* double mutant. Values are given as mean ± SD ($n = 15$). The different letters above the histogram indicate significant differences ($P < 0.05$) by 1-way ANOVA followed by Turkey's multiple comparison test.

in the presence of both the PCF1 and PCF2 transcription factors (Fig. 11C). Although the TGGGCC motif is also a target of PCF1 and PCF2 (Kosugi and Ohashi 1997), neither homodimers of PCF1 or PCF2 nor heterodimers of IPA1 with PCF1 or PCF2 bound to the P1 motif in the *PAL1* promoter (Fig. 11C). The mutation of TGGGCC to AGGGCC ($P1^m$) abolished the binding capacity of IPA1/PCF1/PCF2, confirming that binding to the P1 probe was mediated by the TGGGCC motif. On the other hand, a 66 bp probe containing P2 motif was not recognized by IPA1, at least when the yeast cells were selected on 200 ng/mL Aureobasidin A (AbA), even when PCF1 and PCF2 were present (Supplemental Fig. 12). These results demonstrate that IPA1 binds to the promoter of *PAL1* by forming heterotrimers with PCF1 and PCF2.

To examine whether IPA1 and the 2 TCPs cooperatively regulate *PAL1* expression, we performed transient transcriptional activity assays using rice protoplasts (Fig. 11D). As shown in Fig. 11E, overexpressing *IPA1* or *PCF1* alone only slightly promoted *LUC* expression controlled by the *PAL1* promoter, while overexpressing *PCF2* alone had no noticeable impact on *LUC* expression. In contrast, overexpressing the *IPA1*:*PCF1*:*PCF2* fusion gene markedly increased *LUC* expression (Fig. 11E), suggesting that *in planta*, *PAL1* regulation by IPA1 is based on interactions with the transcription factors PCF1 and PCF2.

We further investigated the biological relevance of *PAL1* as a target of IPA1. Consistent with the role of IPA1 as a transcriptional activator, *PAL1* was significantly upregulated in young panicles of the gain-of-function *ipa1-D* mutant (Jiao et al. 2010; Miura et al. 2010) but downregulated in loss-of-function *ipa1* mutants created by CRISPR/Cas9 in the 'Chunjiang 06' background (Fig. 11, F and G). A total of 15 CRISPR/Cas9 lines were obtained in the T_0 generation, and *ipa1* mutants with homozygous insertions or deletions in the T_1 generation were analyzed. As expected, the loss-of-function *ipa1* mutants showed reduced plant height and increased tiller number and short panicles with fewer branches and grains than the WT (Supplemental Fig. 13). We also generated the *pal1 ipa1-D* double mutant. The *ipa1-D* mutant had larger panicles with more branches and grains, whereas the *pal1* mutant showed much smaller panicles than the WT (Fig. 12, A and B). In the *pal1 ipa1-D* double mutant, the panicle length, primary branch number, secondary branch number, and grain number per panicle were all significantly reduced compared with the *ipa1*-D single mutant. However, these morphological traits were comparable with those of the *pal1* single mutant (Fig. 12, C to F). These results strongly suggest that *PAL1* acts downstream of *IPA1* in controlling rice inflorescence development.

Taken together, these results suggest that IPA1 positively regulates *PAL1* through interactions with PCF1 and PCF2

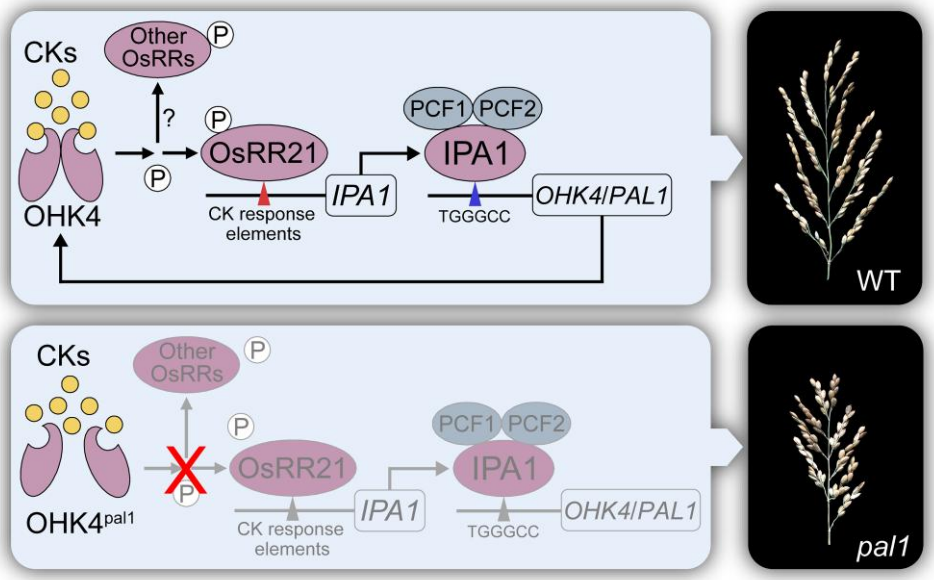

Figure 13. A proposed model for the role of the PAL1-OsRR21-IPA1 circuit in regulating rice inflorescence architecture. The CK receptor OHK4/PAL1 is a positive regulator of rice panicle size that directly binds CKs as a homodimer and transduces the signal to type-B OsRRs through the TCS. OsRR21 is one of the major type-B RRs downstream of OHK4/PAL1 in controlling inflorescence architecture; its activity is dependent on OHK4/PAL1. OsRR21 directly activates *IPA1*. In turn, IPA1 upregulates *OHK4*/*PAL1* by interacting with 2 TCP family transcription factors (PCF1 and PCF2) and binding to the "TGGGCC" motif. Thus, PAL1-OsRR21-IPA1 forms a positive feedback circuit that regulates rice panicle development. The *pal1* mutation disrupts OHK4/PAL1 homodimerization and the perception of CKs and blocks the signal transduction to downstream factors, leading to reduced panicle size.

to control rice panicle size. In turn, the CK signaling mediated by PAL1-OsRR21 directly acts on *IPA1*, forming a positive feedback regulation circuit.

Discussion

Inflorescence architecture, which is primarily determined by meristem activity, plays a fundamental role in controlling rice grain yield. Meristem activity and inflorescence architecture in rice are known to be regulated by the phytohormone CK. However, the genetic/metabolic network between CK signaling and inflorescence development is still not clear.

PAL1 function is associated with meristem activity and inflorescence architecture

In this study, we identified the rice mutant *pal1* whose causal gene encodes the CK receptor OHK4/OsHK4. Similar to its homologs *OHK3*/*OsHK5* and *OHK5*/*OsHK6* (Burr et al. 2020), knockout of *OHK4* resulted in shorter panicles with reduced numbers of branches and grains (Fig. 1, A to G), due to the reduction in SAM and IM activity (Fig. 2). Additionally, we compared the phenotypes of the WT, heterozygous, and homozygous *pal1* mutants, finding no significant differences in plant height or panicle length between WT and the heterozygote (Supplemental Fig. 14, A to E), suggesting that *pal1* is a recessive mutant and that OHK4 has specific functions distinct from those of its homologs. We also created multiple *ohks* mutants by CRISPR/Cas9-mediated gene editing (Supplemental Fig. 15, A and B). Compared with the *ohk4* (*pal1*) single mutant, the plant heights of *ohk3 ohk4* and *ohk4 ohk5* double mutants were slightly but significantly reduced, while the tiller numbers varied. However, the *ohk3 ohk4 ohk5* triple mutants were slender and tiny, with far fewer tillers than the WT (Supplemental Fig. 15, C to E). Likewise, panicle sizes of the *ohk3 ohk4* and *ohk4 ohk5* double mutants were only slightly reduced, but the *ohk3 ohk4 ohk5* triple mutant displayed severe defects in inflorescence size (Supplemental Fig. 15, F to K). These results imply that *OHK3*, *OHK4*, and *OHK5* play at least partially redundant roles in controlling meristem activity and inflorescence architecture.

Several meristem-associated genes were downregulated in the *pal1* mutant (Fig. 3), implying that *PAL1* controls inflorescence size by regulating meristem activity. Among these, *WUS* and *KNOXs* play critical roles in meristem maintenance and differentiation. *CLV*−*WUS* (*CLAVATA*−*WUSCHEL*) feedback signaling in *Arabidopsis* is required for SAM maintenance and is mediated by CK (Schoof et al. 2000; Gordon et al. 2009). The *WUS* promoter can be directly bound by type-B RRs (Dai et al. 2017; Meng et al. 2017; Wang et al. 2017; Zubo et al. 2017; Zhang et al. 2017a; Xie et al. 2018), but whether *OsWUS* is directly regulated by type-B RRs in rice is not clear. In rice, OsWUS is a major regulator of axillary meristem activity and tiller bud formation. In loss-of-function mutants of *OsWUS*, such as *tiller absent1* or *monoclum3*, tiller number is significantly reduced. At the

reproductive stage, the mutation of *OsWUS* mainly caused defects in spikelet development while panicle length was not affected (Lu et al. 2015; Tanaka et al. 2015).

The relationship between CK signaling and *KNOXs* in plants was also revealed long ago (Jasinski et al. 2005; Yanai et al. 2005; Tsuda et al. 2011; Naruse et al. 2018), but the specific regulatory mechanism is still uncertain. The expression of various *KNOX* genes is directly or indirectly regulated by different type-B RRs, which mediate CK receptor signaling. This may explain the downregulation of the *KNOX* gene *OSH3* and *OSH15* in the *pal1* mutant rather than *OSH1*, which is usually used as a meristem marker. In our attempt to test whether the *OSH3* and *OSH15* promoter can be directly bound by some type-B RRs, we used OsRR21 as a prey in a Y1H assay. OsRR21 failed to bind to CK response elements in the *OSH3* and *OSH15* promoters (Supplemental Fig. 16, A to D), even though *OSH15* has been reported to regulate rice panicle length and grain number (Wang et al. 2022). These results imply that the altered expression of these genes in the *pal1* mutant could be due to an indirect effect or that other type-B RRs may act between *PAL1* and *KNOXs*. In fact, besides OsRR21, several other type-B RRs such as OsRR22 and OsRR23 have been reported to regulate rice panicle size (Worthen et al. 2019). We speculate that OsRR22 and OsRR23 might also be type-B RRs that function downstream of PAL1. Additionally, OsRR26 also bound to the *IPA1* promoter, although the biological function of OsRR26 in regulating rice panicle architecture is currently unclear. Therefore, further studies on uncovering the PAL1-OsRR22/OsRR23/OsRR26 CK pathway and their downstream meristem-confined genes will provide more insight into how PAL1 regulates rice panicle size.

PAL1, *OsRR21*, and *IPA1* form a positive feedback circuit that regulates rice panicle development

IPA1 plays a critical role in controlling meristem activity and panicle size (Jiao et al. 2010; Miura et al. 2010; Wang et al. 2015; Zhang et al. 2017b). Several plant hormone-related genes were shown to be regulated by IPA1, such as *LOG*, pointing to a potential link between IPA1 and CK signaling (Lu et al. 2013). Our studies revealed that IPA1 positively regulates *PAL1*, which encodes the CK receptor OHK4. IPA1 binds to the *PAL1* promoter through interactions with PCF1 and PCF2 (Fig. 11C), which belong to the TCP-P family of proteins that affect plant growth and propagation (Martín-Trillo and Cubas 2010). PCF1 and PCF2 homo- or heterodimers can also target the TGGGCC/T motif and regulate the meristematic tissue-specific expression of rice proliferating cell nuclear antigen (*PCNA*) genes (Kosugi and Ohashi 1997). Under our experimental conditions, neither homodimers of PCF1 or PCF2 nor heterodimers of IPA1 with PCF1 or PCF2 exhibited affinity to the *PAL1* promoter, pointing to the critical role of heterotrimers of IPA1, PCF1, and PCF2 in regulating *PAL1* expression.

Recent studies have uncovered a link between CK signaling and *SPLs* in controlling the juvenile-to-adult transition in *Arabidopsis*. Regulation of the vegetative phase change by CK relies on *SPLs*, but no change in *SPL* expression was detected after CK treatment (Werner et al. 2021). Our study also revealed a relationship between CK and *OsSPL14*/*IPA1* in rice. Intriguingly, we found that exogenous CK treatment induced the expression of *IPA1* and that type-B OsRR21 directly upregulates *IPA1*, suggesting positive feedback regulation between *IPA1* and CK signaling (Fig. 13). We found that OsRR22 and OsRR26 could also bind directly to the *IPA1* promoter (Supplemental Fig. S7). Therefore, we cannot rule out the possibility that other type-B RRs may also be involved in *PAL1-IPA1* regulatory circuit. On the other hand, overexpression of *OsRR21* in the *pal1* mutant only largely rescued the panicle phenotype of the *pal1* mutant and not its other phenotypes (Fig. 10), indicating that besides the *PAL1-OsRR21-IPA1* regulatory circuit, there could be other key factors downstream of *PAL1* that contribute to the small panicle size in the *pal1* mutant. Therefore, it would be worth identifying additional CK signaling components that act downstream of *PAL1* and their target genes involved in rice panicle development.

The integrity of the α-helical stalk in OHK4 (PAL1) is required for receptor dimerization and CK-binding capacity

Structural analysis showed that the extracytosolic sensory module of a typical CK receptor can form a homodimer in which the membrane-distal part of the long α-helical stalk forms the dimer interface (Hothorn et al. 2011; Steklov et al. 2013; Liu et al. 2015; Arkhipov et al. 2019). The long α-helical stalk is highly conserved in its membrane-distal region and could contain 2 PAS subdomains due to its rigidity enhanced by disulfide bonds (Hothorn et al. 2011; Steklov et al. 2013). However, its biological function has been unclear.

In our case, the D86th and Q87th deletions located in the center of this long α-helix abolished the dimerization of the receptor sensory modules and resulted in a drastic decrease in CK-binding capacity (Fig. 6). This is particularly intriguing, as the D86-Q87 deletion does not directly touch either the ligand-binding PAS subdomain or the dimerization interface, at least in the dimer conformation that is known from the AHK4 crystal structure and was obtained by modeling the OHK4/PAL1 sensory module. Two possible scenarios derived from homology and ab initio modeling could explain the deletion effects. In the first scenario, the D86-Q87 deletion may result in a rupture in the α-helix stalk and the formation of 2 shorter α-helices connected by a short loop (Fig. 6A). Thus, the long α-helix loses its rigidity and due to the loop formed in the deletion site, the membrane-distal parts bearing the dimerization surface can deviate from the main axis, which can impair the mutual recognition and interaction of the sensor module dimer subunits. The relative mobility of the sensor module placing the PAS domain too close to the

proximal PAS-like domain may alter the initial conformation, which was optimal for the entry and high-affinity binding of CK.

Alternatively, perhaps the long α-helix recovers along the entire stalk, but its membrane-distal region above the deletion zone rotates around its axis at an angle corresponding to the 2 residues removed from the helix. As a result, the strongly conserved amino acid residues involved in dimerization move out of the interface. Therefore, it is no longer possible to form conserved bonds that play key roles in sensor module dimerization. The amino acid composition of the surface of the α-helix interacting with the ligand-binding PAS domain changes as well, which can provoke conformational changes in the latter, impeding the CK–receptor interaction. Overall, our results underline the importance of the indirect effects of the long α-helix on receptor–ligand-binding activity.

PAL1 is required for maintaining CK homeostasis

The deficiency of *in planta* CK signaling has been shown to alter CK homeostasis. In *Arabidopsis*, double or triple CK receptor mutants show significant increases in CK contents, while single receptor mutants show similar or even reduced CK levels compared with WT, as exemplified by the decrease in iP levels in the *ahk2-5* and *cre1-2* mutants (Riefler et al. 2006). Another study with the moss *Physcomitrium patens* revealed that the contents of active CKs including iP, tZ, and dihydrozeatin (DHZ) were not markedly changed either in double or triple receptor mutants (von Schwartzenberg et al. 2016). These studies demonstrated a diverse impact of CK signaling on CK homeostasis between flowering plants and bryophytes. In rice, we detected a drastic decrease in CK levels in the *pal1* mutant (Fig. 8A), which is similar to that observed in *Arabidopsis ahk2-5* and *cre1-2* mutants. Thus, we propose that *Arabidopsis* and rice may share a conserved but yet unknown feedback reaction to the inactivation of CK receptors. Genes involved in CK biosynthesis and degradation were all upregulated in the *pal1* mutant (Fig. 8, B to G). Notably, the *OsCKX2* transcript level was drastically increased in the mutant (Fig. 8D), suggesting that the decrease in CK content in the *pal1* mutant results from CK degradation rather than reduced CK biosynthesis.

The hyperaccumulation of *OsCKX2* transcript in the *pal1* mutant suggests that *OsCKX2* could be a crucial downstream gene of *PAL1*. However, this result is unexpected, since *CKXs* were reported to be induced by CK, and some of them can be directly activated by type-B RRs (Werner et al. 2006; Gao et al. 2014). One possible explanation for the upregulation of *OsCKX2* is that the loss-of-function mutation of the receptor caused an increase in CK biosynthesis as a negative feedback response aiming to restore the signaling level. In fact, *OsIPT1* and *OsIPT4* were already reported to be negatively regulated by CK signaling (Sakamoto et al. 2006). The increased expression of *OsIPTs* and *LOGs* in the *pal1* mutant may trigger rapid CK accumulation, which in turn provokes the strong induction and persistent expression of *OsCKXs* (particularly *OsCKX2*), ultimately leading to reduced CK content. This may cause a further reduction of CK signaling, defective meristems, and underdevelopment of inflorescences. To validate whether *OsCKX2* acts downstream of *PAL1*, a double mutant of *PAL1* and *OsCKX2* needs to be created in the future. Additionally, studies using diverse *ohk* mutants may provide new insight into the interconnection between CK signaling and homeostasis.

Exploring *PAL1* genotypes for improving rice grain yield

Although the mechanism of *PAL1* in controlling inflorescence development was basically deciphered, the potential of *PAL1* for improving rice grain yield remains to be explored. Haplotype analysis using a minicore rice germplasm (524 accessions) from the 3,000 Rice Genomes Project (Wang et al. 2018) revealed plentiful nucleotide diversity of *PAL1*, particularly in the coding sequence (CDS) region. Based on these variations, 3 major haplotypes (Hap1 to Hap3) were identified (Supplemental Fig. 17A). Among these, Hap2 displayed the potential for improving panicle size and yield (Supplemental Fig. 17, B to E). Since the marked effects of CKs on meristem activity and inflorescence architecture have been revealed, more genotypes harboring mutated CK receptor genes should be created, especially gain-of-function variations. To date, only a few gain-of-function mutants for CK receptors have been reported. In *Lotus japonicus*, a mutation in the CK receptor LHK1 triggered spontaneous root nodule organogenesis (Tirichine et al. 2007). In maize, gain-of-function mutations of the CK receptor ZmHK1 altered leaf morphogenesis (Muszynski et al. 2020). In *Arabidopsis*, the *repressor of cytokinin deficiency2* (*rock2*) and *rock3* mutants constitutively transmit CK signals from AHK2 and AHK3 across the membrane, resulting in enlarged flowers and increased seed yield (Bartrina et al. 2017). Another gain-of-function mutation of *AHK3* delayed leaf senescence (Kim et al. 2006). Apart from spontaneous mutations, several gain-of-function versions of AHK were obtained in vitro using a PCR technique (Miwa et al. 2007). Thus, the ability to manipulate the activity of CK receptors opens up broad prospects for increasing the productivity of crops, including rice.

Materials and methods

Plant materials and growth conditions

The *pal1* mutant was isolated from a ^{60}Co γ-ray radiation-treated population of the elite *japonica* rice (*O. sativa*) variety 'Huaidao 5'. Plants were grown in paddy fields in Beijing, Shandong, Jiangsu, and Hainan provinces, China, under natural conditions. To collect samples at the seedling stage, rice seedlings were grown hydroponically in ddH_2O or Yoshida nutrient solution (Coolaber) in a growth chamber. The diurnal cycle was set to 12 h light and 12 h dark (28°C) with ∼150 μmol $m^{-2}s^{-1}$ white light and 60% relative humidity.

Analysis of plant anatomy

For SAM observation, SBs of 14-d-old seedlings of both WT and the *pal1* mutant were treated as previously reported (Ma et al. 2017). SAMs were observed under an LSM700 confocal laser scanning microscope (Zeiss), and SAM sizes were measured using ImageJ. The excitation/emission wavelengths for Hoechst 33342 staining of nuclei were 350/461 nm.

For SEM, young panicles were fixed in 3.5% glutaraldehyde solution, dehydrated, dried, and sputter-coated with gold (Zafar et al. 2020). A scanning electron microscope (Hitachi S3400N) was used for observation, and IM sizes were measured using ImageJ.

Map-based cloning

To generate the F_2 population for mapping, *pal1* was crossed with *indica* rice variety 'Dular'. InDel markers were used for primary and fine mapping. The candidate genes were amplified and sequenced from both the *pal1* mutant and WT. The primers used are listed in Supplemental Tables S1 and S2.

Bioinformatics analysis

Protein sequence alignment was conducted using ClustalW. GENEDOC was used to show consensus sequences and for shading. Three-dimensional modeling of the receptor sensor domain was undertaken based on the X-ray structures of the AHK4 sensor domain (Hothorn et al. 2011). Modeling of the OHK4 receptor sensory module structures (WT and mutant) was accomplished in Modeller 9.20 (Šali and Blundell 1993) using the AutoModel class for comparative modeling. Best models were selected from 200 buildings according to discrete optimized protein energy (DOPE) score (Shen and Sali 2006) calculated by Modeller. Additional structures of the mutated OHK4 sensory module were obtained via ab initio modeling using the IntFOLD5 server (McGuffin et al. 2019). After adding hydrogen atoms, best models were energy-minimized in UCSF Chimera 1.14 (Pettersen et al. 2004) using an AMBER 14SB force field (Maier et al. 2015) with 300 steps of steepest descent and 300 steps of conjugate gradient; step size was 0.02 Å in both cases.

RNA extraction and RT-qPCR

An RNAprep Pure Plant Kit (TIANGEN) and HiScript II Q RT SuperMix (Vazyme) were used for RNA isolation and cDNA synthesis, respectively. RT-qPCR analysis was performed in an Applied Biosystems 7500 Real-Time PCR System with 2 × ChamQ SYBR Color qPCR Master Mix (Vazyme), and the data were calculated using the $2^{-\Delta\Delta Ct}$ quantification method (Livak and Schmittgen 2001). The rice *Ubiquitin* gene was used as an internal control. The primers used are listed in Supplemental Table S3.

Vector construction and plant transformation

To generate the *PAL1* complementation construct, the 8,802 bp genomic DNA fragment of *PAL1* including the 2,525 bp sequence upstream of the start codon was amplified from the WT and cloned into the plant binary vector pCAMBIA1305.1 using an In-Fusion HD Cloning Kit (Clontech). For the promoter-GUS vector, the 2,530 bp promoter sequence of *PAL1* was fused with the *GUS* reporter gene. The TCSn promoter including 2 copies of TCSn1, a mini 35S promoter, and TMV Ω elements was synthesized and subcloned into the pCAMBIA1305.1 vector (Zürcher et al. 2013). To knock out *IPA1* and homologs of *PAL1*, the target of each gene was subcloned into the sgRNA intermediate vector and then cloned into the destination vector pYLCRISPR/Cas9P_{ubi}-H (Ma and Liu 2016). For overexpression of *OsRR21*, the *OsRR21* CDS was cloned into the pCAMBIA1305.1UPFHN vector under the control of the maize *Ubiquitin* promoter. To generate *ProIPA1:7mIPA1-GFP*, the *IPA1* CDS was synonymously mutated using a Q5 Site-Directed Mutagenesis Kit (NEB), fused with *GFP* and driven by the *IPA1* promoter, as described previously (Jiao et al. 2010). The constructs were introduced into rice calli via *Agrobacterium tumefaciens*-mediated transformation (Hiei and Komari 2008). The primers used are listed in Supplemental Table S4.

GUS staining

Different tissues were vacuum-infiltrated for 20 to 30 min in GUS staining buffer (Jefferson et al. 1987). Following incubation in the dark at 37°C for 3 to 12 h, the samples were cleared using an ethanol gradient to remove the chlorophyll and then photographed under a stereomicroscope (Olympus SZX16).

Subcellular localization

The *PAL1* CDS was fused to the N-terminus of GFP and inserted between the CaMV 35S promoter and NOS polyA in pCAMBIA1305.1. The primers used are listed in Supplemental Table S4. The construct was coexpressed with mCherry-HDEL (ER marker) (Nelson et al. 2007) in *N. benthamiana* leaf epidermal cells. The fluorescence of GFP and mCherry was observed under an LSM 700 confocal laser scanning microscope (Zeiss). The excitation/emission wavelengths were 488/507 and 580/610 nm for GFP and mCherry, respectively.

In situ hybridization

For *PAL1*, a 359 bp DNA fragment in the 3′-UTR was amplified and cloned into the pSPT18 vector. The fragment containing the T7 or SP6 promoter was amplified and purified for the synthesis of DIG-labeled sense and anti-sense RNA probes. For other genes, the same method was used. Sample fixation and in situ hybridization were performed as described previously (Coen et al. 1990). The primers used are listed in Supplemental Table S4.

CK response test

To test the responses of seedling roots to CK treatment, WT and *pal1* were grown in ddH_2O supplied with various concentrations of tZ for 10 d in the growth chamber following

2 d of germination at 37°C. For dark treatment, WT and *pal1* were grown in Yoshida nutrient solution (Coolaber) to the 3-leaf stage in the growth chamber following 2 d of germination at 37°C. The middle portions of leaves were cut into 1 cm segments and incubated in the dark for 7 d in ddH_2O supplied with various concentrations of tZ. The chlorophyll was extracted and measured on the 7th day as described previously (Arnon 1949).

CK-binding assay

The cDNA fragments encoding receptor sensory modules (WT and mutant) with adjacent transmembrane segments of OHK4 were inserted into the pB7FWG2 vector (Karimi et al. 2007) where they were fused at the 3′-terminus to the *eGFP* gene by GATEWAY technology (Thermo Scientific). The primers used are listed in Supplemental Table S4. The resulting constructs were transformed into *A. tumefaciens* strain GV3101 and transiently expressed in *N. benthamiana* leaves. Isolation of leaf microsomes and their use to examine CK binding in radioligand assays (using [^{3}H]iP) were performed as described earlier (Lomin et al. 2015, 2018a). GFP quantification was performed using a spectrofluorometer (Shimadzu RF-5301 PC).

Quantification of CKs

CK contents in rice panicles (~0.5 cm) were measured using a polymer monolith microextraction/hydrophilic interaction chromatography/electrospray ionization tandem mass spectrometry method (Liu et al. 2010).

Split-ubiquitin yeast 2-hybrid assay

The *PAL1* CDS was amplified from WT and *pal1* cDNA and cloned into the prey vector pPR3N and bait vector pBT3N. The primers used are listed in Supplemental Table S4. The prey and bait vectors were cotransformed into yeast (*Saccharomyces cerevisiae*) strain NMY51 using a Frozen-EZ Yeast Transformation II kit (Zymo). Yeast media SD/-T/-L and SD/-T/-L/-H/-A (Clontech) were used as permissive and test medium, respectively.

Split-LUC assay

The *PAL1* CDS was amplified from WT and the *pal1* mutant Cdna and then cloned into the pCAMBIA1300-nLUC vector (nLuc, N-terminal LUC) and the pCAMBIA1300-cLUC (cLuc, C-terminal LUC) vector. The split-LUC assay was performed in *N. benthamiana* leaves (Chen et al. 2008). The primers used are listed in Supplemental Table S4.

Y1H

Y1H assays were performed using the Matchmaker Gold Yeast One-Hybrid Library Screening System (Clontech) following the manufacturer's instructions. Probes containing the TGGGCC motif in the *PAL1* promoter and probes containing CK response elements in the *IPA1* and *OSHs* promoters were synthesized (Genewiz) and inserted into the pAbAi vector using T4 ligase (NEB). The resulting pAbAi vector was linearized with *Bst*BI and transformed into yeast strain Y1HGold to generate a bait-specific reporter strain. The CDS of *IPA1*, *PCF1*, *PCF2*, and *OsRRs* were separately cloned into the pGADT7 vector, and these vectors were transformed into the bait-specific reporter strain. The yeast cells were plated on SD/-Leu medium (Clontech) containing a certain concentration of AbA (Coolaber). The probe containing the mutated motif was used as a negative control. Total proteins were extracted from yeast cells using a yeast total protein extraction kit (Solarbio, BC3780), and the expression of all prey proteins (GAL4 AD-IPA1, GAL4 AD-PCF1, and GAL4 AD-PCF2) was detected using anti-GAL4 AD antibody (YM3410, 1:3000, ImmunoWay). The primers used are listed in Supplemental Table S5.

Transcriptional activity assay

To generate the effector constructs, the CDSs of *IPA1*, *PCF1*, *PCF2*, or the *IPA1*:*PCF1*:*PCF2* fusion gene were cloned into the pAN580 vector, while the CDSs of *OsRR21*, *OsRR22*, and *OsRR23* were cloned into the pCAMBIA1305.1 vector. The 1.8 kb promoter fragment of *PAL1* and *IPA1* was cloned into the pGreenII 0800 vector to drive the *LUC* reporter gene. The primers used are listed in Supplemental Table S6. For the transcriptional activity assay of IPA1, PCF1, and PCF2, the corresponding reporters and effectors were coexpressed in rice protoplasts as reported in Yoo et al. (2007), while for the OsRR transcriptional activity assay, the corresponding reporters and effectors were coexpressed in *N. benthamiana* leaves as described above. The Dual-Luciferase Reporter Assay System (Promega) was used to measure LUC and Renilla (REN) activity.

ChIP-qPCR assay

The ChIP-qPCR assay was performed as described previously (Fang et al. 2021). Approximately 1.5 g seedling shoots of the *ProUBI*:*HA-OsRR21* overexpression and *ProIPA1*:*7mIPA1-GFP* plants were cross-linked with 1% (*v*/*v*) formaldehyde and ground into a fine powder in liquid nitrogen. The chromatin complexes were isolated and sonicated into 0.2 to 1.0 kb fragments and incubated with anti-HA (ab9110, 1:500, Abcam) or anti-GFP (598, 1:500, MBL) antibodies. IgG (AC005, 1:500, ABclonal) serum was used as a negative control. The immunocomplexes were collected using Protein A agarose beads (Coolaber). Finally, the immunoprecipitated DNA was recovered after washing, elution, and reversing the cross-linking. The extracted DNA samples from input, ChIP with antibody, and ChIP with IgG serum were used as the template for ChIP-qPCR. The absolute enrichment of specific regions in the *PAL1* and *IPA1* promoters was quantified as the ratio of ChIP to input. The relative enrichment was then calculated by dividing the absolute enrichment value of ChIP with antibody by that of ChIP with IgG serum. The primers used are listed in Supplemental Table S7.

In vivo phosphorylation assay

The CDS of the OsRR21 RR domain was cloned into the pRT105-myc vector (the primers used are listed in Supplemental Table S4) and transformed into rice protoplasts. After overnight incubation, 100 μM cycloheximide (CHX) and 5 μM 6-BA were added to the protoplasts, followed by one more hour of incubation. The protoplasts were then collected gently and lysed in extraction buffer (10 mM Tris-HCl, pH 7.5, 150 mM NaCl, 0.5% Nonidet P-40) supplemented with 1 mM phenylmethanesulfonyl fluoride (PMSF), 1% protease inhibitor cocktail (Roche). To confirm phosphorylation, 1% CIP cocktail (Roche) was applied. After 15 min incubation on ice, the lysate was centrifuged at 12,000 rpm and 4°C for 5 min, and the supernatant was used for SDS–PAGE. To generate the Phos-tag gel, the SDS–PAGE gel was supplemented with 200 μM $MnCl_2$ and 100 μM Phos-tag (WAKO). After electrophoresis, the gel was treated with EDTA to remove $MnCl_2$, as described in the Phos-tag handbook. For immunoblotting, anti-myc antibody (M192-3, 1:4000, MBL) and goat antir-rabbit and mouse IgG-HRP (M21003, 1:3,000, Abmart) were used. The same samples were used for routine SDS–PAGE and immunoblot analysis to check for equal loading.

Haplotype analysis

The genotype data of *PAL1* in 524 rice accessions were obtained from the 3,000 Rice Genomes Project (https://www.ncbi.nlm.nih.gov/sra/?term=PRJEB6180) (Wang et al. 2018). The heterozygous alleles were eliminated. The panicle traits were measured after harvest.

Statistical analysis

The statistical significance of differences was evaluated by Student's *t* test and 1-way ANOVA followed by Turkey's multiple comparison test using GraphPad Prism 8 (Supplemental Data Set S1). "*" and "**" indicate the significant differences at $P < 0.05$ and $P < 0.01$, respectively. The different letters above the histogram indicate the differences at $P < 0.05$.

Accession numbers

The mentioned genes and their sequence information can be found in Rice Genome Annotation Project (http://rice.plantbiology.msu.edu/) under the following accession numbers: *OsHK4*/*OHK4* (*LOC_Os03g50860*, *MW533262*), *OHK3*/*OsHK5* (*LOC_Os10g21810*), and *OHK5*/*OsHK6* (*LOC_Os02g50480*). The accession numbers of other genes are listed in Supplemental Tables S3 and S5.

Acknowledgments

We thank Prof. Zhikang Li, Jianlong Xu, and Zefu Lu (Institute of Crop Sciences, Chinese Academy of Agricultural Sciences) for providing the 524 rice accessions and IPA1 binding profile, Prof. Hang He (Peking University) for haplotype analysis, and Prof. Xiaojin Luo (Fudan University) for providing the field to grow transgenic plants.

Y.C., J.F., J.S., Y.S., J.Z., A.K., C.-M.L., and X.L. are affiliated with the State Key Laboratory of Crop Gene Resources and Breeding, Institute of Crop Sciences, Chinese Academy of Agricultural Sciences, Beijing 100081, China. E.M.S., S.N.L., D.V.A. and G.A.R. are affiliated with the Timiryazev Institute of Plant Physiology, Russian Academy of Sciences, Moscow 127276, Russia. S.Y. is affiliated with the Institute of Wetland Agriculture and Ecology, Shandong Academy of Agricultural Sciences, Jinan 250100, China. X.Y. and C.-M.L. are affiliated with the Key Laboratory of Plant Molecular Physiology, Institute of Botany, Chinese Academy of Sciences, Beijing 100093, China.

Author contributions

X.L. and G.A.R. designed the experiments. Y.C., J.F., E.M.S., S.N.L., J.S., Y.S., J.Z., A.K., S.Y., X.Y., C.-M.L., and D.V.A. performed the experiments. Y.C. and E.M.S. analyzed the data. Y.C. wrote the manuscript. X.L. and G.A.R. revised the manuscript and supervised the whole study.

Supplemental data

The following materials are available in the online version of this article.

Supplemental Figure S1. Morphological characterization of the *pal1* plant.

Supplemental Figure S2. Sequence alignment of the CK receptor family.

Supplemental Figure S3. Allelic mutants of *PAL1*.

Supplemental Figure S4. Expression pattern of *PAL1* revealed by GUS staining assay.

Supplemental Figure S5. Transient expression of PAL1 protein in *N. benthamiana* leaves and ligand-binding assay.

Supplemental Figure S6. Comparison of the expression levels of type-A and type-B RR genes between WT and *pal1*.

Supplemental Figure S7. Y1H assay for binding of OsRR22, OsRR23, and OsRR26 to the *IPA1* promoter.

Supplemental Figure S8. Phenotypes of *OsRR21* overexpression plants in the WT background.

Supplemental Figure S9. Expression and phosphorylation of OsRR21 in rice protoplasts.

Supplemental Figure S10. Phenotypes of *ProIPA1:7mIPA1-GFP* plants.

Supplemental Figure S11. Expression of prey proteins in a Y1H assay.

Supplemental Figure S12. Y1H assay showing that IPA1 might be unable to bind P2.

Supplemental Figure S13. Phenotypes of *IPA1* knockout plants.

Supplemental Figure S14. Morphological comparison of plants and panicles among WT, +/*pal1*, and *pal1* reveals that *pal1* is a recessive mutant.

Supplemental Figure S15. Phenotypes of the multiple mutants of *ohks*.

Supplemental Figure S16. Y1H assays showing that OsRR21 is unable to bind to the promoters of *OSH3* and *OSH15*.

Supplemental Figure S17. Haplotype analysis of *PAL1*.

Supplemental Table S1. Primers used for gene mapping.

Supplemental Table S2. Primers used for the amplification of *PAL1* genomic DNA.

Supplemental Table S3. Primers used for RT-qPCR.

Supplemental Table S4. Primers used for vector construction.

Supplemental Table S5. Primers used for Y1H assays.

Supplemental Table S6. Primers used for the transcriptional activity assays.

Supplemental Table S7. Primers used for ChIP-qPCR.

Supplemental Data Set 1. Summary of statistical tests.

Funding

Studies carried out in China were supported by the National Key Research and Development Program of China (2022YFD1200103), the Agricultural Variety Improvement Project of Shandong Province (2021LZGC020), the National Natural Science Foundation of China (32300278), the China Postdoctoral Science Foundation (2022M723455), and the Agricultural Science and Technology Innovation Program of the Chinese Academy of Agricultural Sciences. Studies carried out in Russia were partially supported by the subsidy of the Ministry of Science and Higher Education of the Russian Federation (theme no. 122042700043-9).

Conflict of interest statement. None declared.

Data availability

The data underlying this article are available in the article and in its online supplementary material.

References

Arkhipov DV, Lomin SN, Myakushina YA, Savelieva EM, Osolodkin DI, Romanov GA. Modeling of protein-protein interactions in cytokinin signal transduction. Int J Mol Sci. 2019:**20**(9):2096. https://doi.org/10.3390/ijms20092096

Arnon DI. Copper enzymes in isolated chloroplasts: polyphenoloxidase in *Beta vulgaris*. Plant Physiol. 1949:**24**(1):1–15. https://doi.org/10.1104/pp.24.1.1

Ashikari M, Sakakibara H, Lin S, Yamamoto T, Takashi T, Nishimura A, Angeles ER, Qian Q, Kitano H, Matsuoka M. Cytokinin oxidase regulates rice grain production. Science 2005:**309**(5735):741–745. https://doi.org/10.1126/science.1113373

Bartrina I, Jensen H, Novák O, Strnad M, Werner T, Schmülling T. Gain-of-function mutants of the cytokinin receptors AHK2 and AHK3 regulate plant organ size, flowering time and plant longevity. Plant Physiol. 2017:**173**(3):1783–1797. https://doi.org/10.1104/pp.16.01903

Burr CA, Sun J, Yamburenko MV, Willoughby A, Hodgens C, Boeshore SL, Elmore A, Atkinson J, Nimchuk ZL, Bishopp A, et al. The HK5 and HK6 cytokinin receptors mediate diverse developmental pathways in rice. Development 2020:**147**(20):dev191734. https://doi.org/10.1242/dev.191734

Caesar K, Thamm AM, Witthöft J, Elgass K, Huppenberger P, Grefen C, Horak J, Harter K. Evidence for the localization of the *Arabidopsis* cytokinin receptors AHK3 and AHK4 in the endoplasmic reticulum. J Exp Bot. 2011:**62**(15):5571–5580. https://doi.org/10.1093/jxb/err238

Chang L, Ramireddy E, Schmülling T. Lateral root formation and growth of *Arabidopsis* is redundantly regulated by cytokinin metabolism and signalling genes. J Exp Bot. 2013:**64**(16):5021–5032. https://doi.org/10.1093/jxb/ert291

Chen H, Zou Y, Shang Y, Lin H, Wang Y, Cai R, Tang X, Zhou J. Firefly luciferase complementation imaging assay for protein-protein interactions in plants. Plant Physiol. 2008:**146**(2):368–376. https://doi.org/10.1104/pp.107.111740

Choi J, Lee J, Kim K, Cho M, Ryu H, An G, Hwang I. Functional identification of *OsHk6* as a homotypic cytokinin receptor in rice with preferential affinity for iP. Plant Cell Physiol. 2012:**53**(7):1334–1343. https://doi.org/10.1093/pcp/pcs079

Chun Y, Kumar A, Li X. Genetic and molecular pathways controlling rice inflorescence architecture. Front Plant Sci. 2022:**13**:1010138. https://doi.org/10.3389/fpls.2022.1010138

Coen ES, Romero JM, Doyle S, Elliott R, Murphy G, Carpenter R. Floricaula: a homeotic gene required for flower development in *Antirrhinum majus*. Cell 1990:**63**(6):1311–1322. https://doi.org/10.1016/0092-8674(90)90426-F

D'Agostino IB, Deruère J, Kieber JJ. Characterization of the response of the *Arabidopsis* response regulator gene family to cytokinin. Plant Physiol. 2000:**124**(4):1706–1717. https://doi.org/10.1104/pp.124.4.1706

Dai X, Liu Z, Qiao M, Li J, Li S, Xiang F. ARR12 promotes *de novo* shoot regeneration in *Arabidopsis thaliana* via activation of *WUSCHEL* expression. J Integr Plant Biol. 2017:**59**(10):747–758. https://doi.org/10.1111/jipb.12567

Ding W, Tong H, Zheng W, Ye J, Pan Z, Zhang B, Zhu S. Isolation, characterization and transcriptome analysis of a cytokinin receptor mutant *Osckt1* in rice. Front Plant Sci. 2017:**8**:88. https://doi.org/10.3389/fpls.2017.00088

Fang J, Guo T, Xie Z, Chun Y, Zhao J, Peng L, Zafar SA, Yuan S, Xiao L, Li X. The URL1-ROC5-TPL2 transcriptional repressor complex represses the *ACL1* gene to modulate leaf rolling in rice. Plant Physiol. 2021:**185**(4):1722–1744. https://doi.org/10.1093/plphys/kiaa121

Gao R, Stock AM. Biological insights from structures of two-component proteins. Annu Rev Microbiol. 2009:**63**(1):133–154. https://doi.org/10.1146/annurev.micro.091208.073214

Gao S, Fang J, Xu F, Wang W, Sun X, Chu J, Cai B, Feng Y, Chu C. CYTOKININ OXIDASE/DEHYDROGENASE4 integrates cytokinin and auxin signaling to control rice crown root formation. Plant Physiol. 2014:**165**(3):1035–1046. https://doi.org/10.1104/pp.114.238584

Gordon SP, Chickarmane VS, Ohno C, Meyerowitz EM. Multiple feedback loops through cytokinin signaling control stem cell number within the *Arabidopsis* shoot meristem. Proc Natl Acad Sci USA. 2009:**106**(38):16529–16534. https://doi.org/10.1073/pnas.0908122106

Halawa M, Cortleven A, Schmülling T, Heyl A. Characterization of CHARK, an unusual cytokinin receptor of rice. Sci Rep. 2021:**11**(1):1722. https://doi.org/10.1038/s41598-020-80223-2

Heyl A, Schmülling T. Cytokinin signal perception and transduction. Curr Opin Plant Biol. 2003:**6**(5):480–488. https://doi.org/10.1016/S1369-5266(03)00087-6

Hosoda K, Imamura A, Katoh E, Hatta T, Tachiki M, Yamada H, Mizuno T, Yamazaki T. Molecular structure of the GARP family of plant Myb-related DNA binding motifs of the Arabidopsis response regulators. Plant Cell. 2002:**14**(9):2015–2029. https://doi.org/10.1105/tpc.002733

Hiei Y, Komari T. Agrobacterium-mediated transformation of rice using immature embryos or calli induced from mature seed. Nat Protoc. 2008:**3**(5):824–834. https://doi.org/10.1038/nprot.2008.46

Higuchi M, Pischke MS, Mähönen AP, Miyawaki K, Hashimoto Y, Seki M, Kobayashi M, Shinozaki K, Kato T, Tabata S, et al. *In planta* functions of the Arabidopsis cytokinin receptor family. Proc Natl Acad Sci USA. 2004:**101**(23):8821–8826. https://doi.org/10.1073/pnas.0402887101

Hothorn M, Dabi T, Chory J. Structural basis for cytokinin recognition by *Arabidopsis thaliana* histidine kinase 4. Nat Chem Biol. 2011:**7**(11):766–768. https://doi.org/10.1038/nchembio.667

Huang X, Qian Q, Liu Z, Sun H, He S, Luo D, Xia G, Chu C, Li J, Fu X. Natural variation at the *DEP1* locus enhances grain yield in rice. Nature Genet. 2009:**41**(4):494–497. https://doi.org/10.1038/ng.352

Hutchison CE, Li J, Argueso C, Gonzalez M, Lee E, Lewis MW, Maxwell BB, Perdue TD, Schaller GE, Alonso JM, et al. The *Arabidopsis* histidine phosphotransfer proteins are redundant positive regulators of cytokinin signaling. Plant Cell. 2006:**18**(11):3073–3087. https://doi.org/10.1105/tpc.106.045674

Ikeda K, Nagasawa N, Nagato Y. *ABERRANT PANICLE ORGANIZATION 1* temporally regulates meristem identity in rice. Dev Biol. 2005:**282**(2):349–360. https://doi.org/10.1016/j.ydbio.2005.03.016

Ikeda-Kawakatsu K, Maekawa M, Izawa T, Itoh J, Nagato Y. *ABERRANT PANICLE ORGANIZATION 2/RFL*, the rice ortholog of Arabidopsis *LEAFY*, suppresses the transition from inflorescence meristem to floral meristem through interaction with *APO1*. Plant J. 2012:**69**(1):168–180. https://doi.org/10.1111/j.1365-313X.2011.04781.x

Ikeda-Kawakatsu K, Yasuno N, Oikawa T, Iida S, Nagato Y, Maekawa M, Kyozuka J. Expression level of *ABERRANT PANICLE ORGANIZATION1* determines rice inflorescence form through control of cell proliferation in the meristem. Plant Physiol. 2009:**150**(2):736–747. https://doi.org/10.1104/pp.109.136739

Inoue T, Higuchi M, Hashimoto Y, Seki M, Kobayashi M, Kato T, Tabata S, Shinozaki K, Kakimoto T. Identification of CRE 1 as a cytokinin receptor from Arabidopsis. Nature 2001:**409**(6823):1060–1063. https://doi.org/10.1038/35059117

Ito Y, Kurata N. Identification and characterization of cytokinin-signalling gene families in rice. Gene 2006:**382**:57–65. https://doi.org/10.1016/j.gene.2006.06.020

Jain M, Tyagi AK, Khurana JP. Molecular characterization and differential expression of cytokinin-responsive type-A response regulators in rice (*Oryza sativa*). BMC Plant Biol. 2006:**6**(1):1. https://doi.org/10.1186/1471-2229-6-1

Jasinski S, Piazza P, Craft J, Hay A, Woolley L, Rieu I, Phillips A, Hedden P, Tsiantis M. KNOX action in *Arabidopsis* is mediated by coordinate regulation of cytokinin and gibberellin activities. Curr Biol. 2005:**15**(17):1560–1565. https://doi.org/10.1016/j.cub.2005.07.023

Jefferson RA, Kavanagh TA, Bevan MW. GUS fusions: beta-glucuronidase as a sensitive and versatile gene fusion marker in higher plants. EMBO J. 1987:**6**(13):3901–3907. https://doi.org/10.1002/j.1460-2075.1987.tb02730.x

Jiang G-Q, Yao X-F, Liu C-M. A simple CELI endonuclease-based protocol for genotyping both SNPs and InDels. Plant Mol Bio Rep. 2013:**31**(6):1325–1335. https://doi.org/10.1007/s11105-013-0606-z

Jiao Y, Wang Y, Xue D, Wang J, Yan M, Liu G, Dong G, Zeng D, Lu Z, Zhu X, et al. Regulation of *OsSPL14* by OsmiR156 defines ideal plant architecture in rice. Nature Genet. 2010:**42**(6):541–544. https://doi.org/10.1038/ng.591

Kakimoto T. Perception and signal transduction of cytokinins. Annu. Rev. Plant Biol. 2003:**54**(1):605–627. https://doi.org/10.1146/annurev.arplant.54.031902.134802

Karimi M, Depicker A, Hilson P. Recombinational cloning with plant GATEWAY vectors. Plant Physiol. 2007:**145**(4):1144–1154. https://doi.org/10.1104/pp.107.106989

Kim HJ, Ryu H, Hong SH, Woo HR, Lim PO, Lee IC, Sheen J, Nam HG, Hwang I. Cytokinin-mediated control of leaf longevity by AHK3 through phosphorylation of ARR2 in *Arabidopsis*. Proc Natl Acad Sci USA. 2006:**103**(3):814–819. https://doi.org/10.1073/pnas.0505150103

Komatsu M, Maekawa M, Shimamoto K, Kyozuka J. The *LAX1* and *FRIZZY PANICLE 2* genes determine the inflorescence architecture of rice by controlling rachis-branch and spikelet development. Dev Biol. 2001:**231**(2):364–373. https://doi.org/10.1006/dbio.2000.9988

Komatsu K, Maekawa M, Ujiie S, Satake Y, Furutani I, Okamoto H, Shimamoto K, Kyozuka J. LAX and SPA: major regulators of shoot branching in rice. Proc Natl Acad Sci USA. 2003:**100**(20):11765–-11770. https://doi.org/10.1073/pnas.1932414100

Kosugi S, Ohashi Y. PCF1 and PCF2 specifically bind to *cis* elements in the rice proliferating cell nuclear antigen gene. Plant Cell. 1997:**9**(9):1607–1619. https://doi.org/10.1105/tpc.9.9.1607

Kurakawa T, Ueda N, Maekawa M, Kobayashi K, Kojima M, Nagato Y, Sakakibara H, Kyozuka J. Direct control of shoot meristem activity by a cytokinin-activating enzyme. Nature 2007:**445**(7128):652–655. https://doi.org/10.1038/nature05504

Laskowski RA, Jabłońska J, Pravda L, Vařeková RS, Thornton JM. PDBsum: structural summaries of PDB entries. Protein Sci. 2018:**27**(1):129–134. https://doi.org/10.1002/pro.3289

Laskowski RA, MacArthur MW, Moss DS, Thornton JM. PROCHECK—a program to check the stereochemical quality of protein structures. J Appl Crystallogr. 1993:**26**(2):283–291. https://doi.org/10.1107/S0021889892009944

Li M, Tang D, Wang K, Wu X, Lu L, Yu H, Gu M, Yan C, Cheng Z. Mutations in the F-box gene *LARGER PANICLE* improve the panicle architecture and enhance the grain yield in rice. Plant Biotechnol J. 2011:**9**(9):1002–1013. https://doi.org/10.1111/j.1467-7652.2011.00610.x

Li S, Zhao B, Yuan D, Duan M, Qian Q, Tang L, Wang B, Liu X, Zhang J, Wang J, et al. Rice zinc finger protein DST enhances grain production through controlling *Gn1a/OsCKX2* expression. Proc Natl Acad Sci USA. 2013:**110**(8):3167–3172. https://doi.org/10.1073/pnas.1300359110

Liu YC, Machuca MA, Beckham SA, Gunzburg MJ, Roujeinikova A. Structural basis for amino-acid recognition and transmembrane signalling by tandem Per-Arnt-Sim (tandem PAS) chemoreceptor sensory domains. Acta Crystallogr D Biol Crystallogr. 2015:**71**(10):2127–2136. https://doi.org/10.1107/S139900471501384X

Liu Z, Wei F, Feng YQ. Determination of cytokinins in plant samples by polymer monolith microextraction coupled with hydrophilic interaction chromatography-tandem mass spectrometry. Anal Methods. 2010:**2**(11):1676–1685. https://doi.org/10.1039/c0ay00334d

Livak KJ, Schmittgen TD. Analysis of relative gene expression data using real-time quantitative PCR and the 2-ΔΔCt method. Methods 2001:**25**(4):402–408. https://doi.org/10.1006/meth.2001.1262

Lomin SN, Krivosheev DM, Steklov MY, Arkhipov DV, Osolodkin DI, Schmülling T, Romanov GA. Plant membrane assays with cytokinin receptors underpin the unique role of free cytokinin bases as biologically active ligands. J Exp Bot. 2015:**66**(7):1851–1863. https://doi.org/10.1093/jxb/eru522

Lomin SN, Myakushina YA, Arkhipov DV, Leonova OG, Popenko VI, Schmülling T, Romanov GA. Studies of cytokinin receptor-phosphotransmitter interaction provide evidences for the initiation of cytokinin signalling in the endoplasmic reticulum. Funct Plant Biol. 2018b:**45**(2):192–202. https://doi.org/10.1071/FP16292

Lomin SN, Myakushina YA, Kolachevskaya OO, Getman IA, Arkhipov DV, Savelieva EM, Osolodkin DI, Romanov GA. Cytokinin perception in potato: new features of canonical players. J Exp Bot. 2018a:**69**(16):3839–3853. https://doi.org/10.1093/jxb/ery199

Lomin SN, Yonekura-Sakakibara K, Romanov GA, Sakakibara H. Ligand binding properties and subcellular localization of maize cytokinin receptors. J Exp Bot. 2011:**62**(14):5149–5159. https://doi.org/10.1093/jxb/err220

Long JA, Moan EI, Medford JI, Barton MK. A member of the KNOTTED class of homeodomain proteins encoded by the *STM* gene of *Arabidopsis*. Nature 1996:**379**(6560):66–69. https://doi.org/10.1038/379066a0

Lu Z, Shao G, Xiong J, Jiao Y, Wang J, Liu G, Meng X, Liang Y, Xiong G, Wang Y, et al. *MONOCULM 3*, an ortholog of *WUSCHEL* in rice, is required for tiller bud formation. J Genet Genomics. 2015:**42**(2):71–78. https://doi.org/10.1016/j.jgg.2014.12.005

Lu Z, Yu H, Xiong G, Wang J, Jiao Y, Liu G, Jing Y, Meng X, Hu X, Qian Q, et al. Genome-wide binding analysis of the transcription activator IDEAL PLANT ARCHITECTURE1 reveals a complex network regulating rice plant architecture. Plant Cell. 2013:**25**(10):3743–3759. https://doi.org/10.1105/tpc.113.113639

Ma W, Wu F, Sheng P, Wang X, Zhang Z, Zhou K, Zhang H, Hu J, Lin Q, Cheng Z, et al. The LBD12-1 transcription factor suppresses apical meristem size by repressing *Argonaute 10* expression. Plant Physiol. 2017:**173**(1):801–811. https://doi.org/10.1104/pp.16.01699

Ma X, Liu YG. CRISPR/Cas9-based multiplex genome editing in monocot and dicot plants. Curr Protoc Mol Biol. 2016:**115**(1):31.6.1–-31.6.21. https://doi.org/10.1002/cpmb.10

Maier JA, Martinez C, Kasavajhala K, Wickstrom L, Hauser KE, Simmerling C. ff14SB: improving the accuracy of protein side chain and backbone parameters from ff99SB. J Chem Theory Comput. 2015:**11**(8):3696–3713. https://doi.org/10.1021/acs.jctc.5b00255

Martín-Trillo M, Cubas P. TCP genes: a family snapshot ten years later. Trends Plant Sci. 2010:**15**(1):31–39. https://doi.org/10.1016/j.tplants.2009.11.003

McGuffin LJ, Adiyaman R, Maghrabi AHA, Shuid AN, Brackenridge DA, Nealon JO, Philomina LS. IntFOLD: an integrated web resource for high performance protein structure and function prediction. Nucleic Acids Res. 2019:**47**(W1):W408–W413. https://doi.org/10.1093/nar/gkz322

Meng W, Cheng ZJ, Sang YL, Zhang MM, Rong XF, Wang ZW, Tang YY, Zhang XS. Type-B ARABIDOPSIS RESPONSE REGULATORs specify the shoot stem cell niche by dual regulation of *WUSCHEL*. Plant Cell. 2017:**29**(6):1357–1372. https://doi.org/10.1105/tpc.16.00640

Miura K, Ikeda M, Matsubara A, Song XJ, Ito M, Asano K, Matsuoka M, Kitano H, Ashikari M. *OsSPL14* promotes panicle branching and higher grain productivity in rice. Nature Genet. 2010:**42**(6):545–549. https://doi.org/10.1038/ng.592

Miwa K, Ishikawa K, Terada K, Yamada H, Suzuki T, Yamashino T, Mizuno T. Identification of amino acid substitutions that render the Arabidopsis cytokinin receptor histidine kinase AHK4 constitutively active. Plant Cell Physiol. 2007:**48**(12):1809–1814. https://doi.org/10.1093/pcp/pcm145

Müller B, Sheen J. Cytokinin and auxin interaction in root stem-cell specification during early embryogenesis. Nature 2008:**453**(7198):1094–1097. https://doi.org/10.1038/nature06943

Muszynski MG, Moss-Taylor L, Chudalayandi S, Cahill J, Del Valle-Echevarria AR, Alvarez-Castro Petefish IA, Sakakibara H, Krivosheev DM, Lomin SN, Romanov GA, et al. The maize *Hairy Sheath Frayed1* (*Hsf1*) mutation alters leaf patterning through increased cytokinin signaling. Plant Cell. 2020:**32**(5):1501–1518. https://doi.org/10.1105/tpc.19.00677

Nakagawa M, Shimamoto K, Kyozuka J. Overexpression of *RCN1* and *RCN2*, rice *TERMINAL FLOWER 1/CENTRORADIALIS* homologs, confers delay of phase transition and altered panicle morphology in rice. Plant J. 2002:**29**(6):743–750. https://doi.org/10.1046/j.1365-313X.2002.01255.x

Naruse M, Takahashi H, Kurata N, Ito Y. Cytokinin-induced expression of *OSH1* in a shoot-regenerating rice callus. Plant Biotechnol. 2018:**35**(3):267–272. https://doi.org/10.5511/plantbiotechnology.18.0614a

Nelson BK, Cai X, Nebenführ A. A multicolored set of *in vivo* organelle markers for co-localization studies in *Arabidopsis* and other plants. Plant J. 2007:**51**(6):1126–1136. https://doi.org/10.1111/j.1365-313X.2007.03212.x

Nishimura C, Ohashi Y, Sato S, Kato T, Tabata S, Ueguchi C. Histidine kinase homologs that act as cytokinin receptors possess overlapping functions in the regulation of shoot and root growth in *Arabidopsis*. Plant Cell. 2004:**16**(6):1365–1377. https://doi.org/10.1105/tpc.021477

Pettersen EF, Goddard TD, Huang CC, Couch GS, Greenblatt DM, Meng EC, Ferrin TE. UCSF Chimera–a visualization system for exploratory research and analysis. J Comput Chem. 2004:**25**(13):1605–1612. https://doi.org/10.1002/jcc.20084

Rao NN, Prasad K, Kumar PR, Vijayraghavan U. Distinct regulatory role for *RFL*, the rice *LFY* homolog, in determining flowering time and plant architecture. Proc Natl Acad Sci USA. 2008:**105**(9):3646–3651. https://doi.org/10.1073/pnas.0709059105

Riefler M, Novak O, Strnad M, Schmülling T. *Arabidopsis* cytokinin receptor mutants reveal functions in shoot growth, leaf senescence, seed size, germination, root development, and cytokinin metabolism. Plant Cell. 2006:**18**(1):40–54. https://doi.org/10.1105/tpc.105.037796

Romanov GA, Lomin SN, Schmülling T. Cytokinin signaling: from the ER or from the PM? That is the question! New Phytol. 2018:**218**(1):41–53. https://doi.org/10.1111/nph.14991

Sakamoto T, Sakakibara H, Kojima M, Yamamoto Y, Nagasaki H, Inukai Y, Sato Y, Matsuoka M. Ectopic expression of KNOTTED1-like homeobox protein induces expression of cytokinin biosynthesis genes in rice. Plant Physiol. 2006:**142**(1):54–62. https://doi.org/10.1104/pp.106.085811

Šali A, Blundell T. Comparative protein modelling by satisfaction of spatial restraints. J Mol Biol. 1993:**234**(3):779–815. https://doi.org/10.1006/jmbi.1993.1626

Schoof H, Lenhard M, Haecker A, Mayer KFX, Jürgens G, Laux T. The stem cell population of *Arabidopsis* shoot meristems is maintained by a regulatory loop between the *CLAVATA* and *WUSCHEL* genes. Cell 2000:**100**(6):635–644. https://doi.org/10.1016/S0092-8674(00)80700-X

Sentoku N, Sato Y, Kurata N, Ito Y, Kitano H, Matsuoka M. Regional expression of the rice KN1-type homeobox gene family during embryo, shoot, and flower development. Plant Cell. 1999:**11**(9):1651–1664. https://doi.org/10.1105/tpc.11.9.1651

Shen MY, Sali A. Statistical potential for assessment and prediction of protein structures. Protein Sci. 2006:**15**(11):2507–2524. https://doi.org/10.1110/ps.062416606

Steklov MY, Lomin SN, Osolodkin DI, Romanov GA. Structural basis for cytokinin receptor signaling: an evolutionary approach. Plant Cell Rep. 2013:**32**(6):781–793. https://doi.org/10.1007/s00299-013-1408-3

Stolz A, Riefler M, Lomin SN, Achazi K, Romanov GA, Schmülling T. The specificity of cytokinin signalling in *Arabidopsis thaliana* is mediated by differing ligand affinities and expression profiles of the receptors. Plant J. 2011:**67**(1):157–168. https://doi.org/10.1111/j.1365-313X.2011.04584.x

Sun L, Zhang Q, Wu J, Zhang L, Jiao X, Zhang S, Zhang Z, Sun D, Lu T, Sun Y. Two rice authentic histidine phosphotransfer proteins, OsAHP1 and OsAHP2, mediate cytokinin signaling and stress responses in rice. Plant Physiol. 2014:**165**(1):335–345. https://doi.org/10.1104/pp.113.232629

Suzaki T, Sato M, Ashikari M, Miyoshi M, Nagato Y, Hirano HY. The gene *FLORAL ORGAN NUMBER1* regulates floral meristem size in rice and encodes a leucine-rich repeat receptor kinase orthologous to *Arabidopsis* CLAVATA1. Development 2004:**131**(22):5649–5657. https://doi.org/10.1242/dev.01441

Tabuchi H, Zhang Y, Hattori S, Omae M, Shimizu-Sato S, Oikawa T, Qian Q, Nishimura M, Kitano H, Xie H, et al. *LAX PANICLE2* of rice encodes a novel nuclear protein and regulates the formation of axillary meristems. Plant Cell. 2011:**23**(9):3276–3287. https://doi.org/10.1105/tpc.111.088765

Tanaka W, Ohmori Y, Ushijima T, Matsusaka H, Matsushita T, Kumamaru T, Kawano S, Hirano HY. Axillary meristem formation in rice requires the *WUSCHEL* ortholog *TILLERS ABSENT1*. Plant Cell. 2015:**27**(4):1173–1184. https://doi.org/10.1105/tpc.15.00074

Taniguchi M, Kiba T, Sakakibara H, Ueguchi C, Mizuno T, Sugiyama T. Expression of *Arabidopsis* response regulator homologs is induced

by cytokinins and nitrate. FEBS Lett. 1998:**429**(3):259–262. https://doi.org/10.1016/S0014-5793(98)00611-5

Tirichine L, Sandal N, Madsen LH, Radutoiu S, Albrektsen AS, Sato S, Asamizu E, Tabata S, Stougaard J. A gain-of-function mutation in a cytokinin receptor triggers spontaneous root nodule organogenesis. Science 2007:**315**(5808):104–107. https://doi.org/10.1126/science.1132397

Tsuda K, Ito Y, Sato Y, Kurata N. Positive autoregulation of a *KNOX* gene is essential for shoot apical meristem maintenance in rice. Plant Cell. 2011:**23**(12):4368–4381. https://doi.org/10.1105/tpc.111.090050

Ueguchi C, Sato S, Kato T, Tabata S. The *AHK4* gene involved in the cytokinin-signaling pathway as a direct receptor molecule in *Arabidopsis thaliana*. Plant Cell Physiol. 2001:**42**(7):751–755. https://doi.org/10.1093/pcp/pce094

von Schwartzenberg K, Lindner AC, Gruhn N, Šimura J, Novák O, Strnad M, Gonneau M, Nogué F, Heyl A. CHASE domain-containing receptors play an essential role in the cytokinin response of the moss *Physcomitrella patens*. J Exp Bot. 2016:**67**(3):667–679. https://doi.org/10.1093/jxb/erv479

Wang H, Tong X, Tang L, Wang Y, Zhao J, Li Z, Liu X, Shu Y, Yin M, Adegoke TV, et al. RLB (RICE LATERAL BRANCH) recruits PRC2-mediated H3K27 tri-methylation on *OsCKX4* to regulate lateral branching. Plant Physiol. 2022:**188**(1):460–476. https://doi.org/10.1093/plphys/kiab494

Wang J, Tian C, Zhang C, Shi B, Cao X, Zhang TQ, Zhao Z, Wang JW, Jiao Y. Cytokinin signaling activates *WUSCHEL* expression during axillary meristem initiation. Plant Cell. 2017:**29**(6):1373–1387. https://doi.org/10.1105/tpc.16.00579

Wang L, Sun S, Jin J, Fu D, Yang X, Weng X, Xu C, Li X, Xiao J, Zhang Q. Coordinated regulation of vegetative and reproductive branching in rice. Proc Natl Acad Sci USA. 2015:**112**(50):15504–15509. https://doi.org/10.1073/pnas.1521949112

Wang W, Mauleon R, Hu Z, Chebotarov D, Tai S, Wu Z, Li M, Zheng T, Fuentes RR, Zhang F, et al. Genomic variation in 3,010 diverse accessions of Asian cultivated rice. Nature 2018:**557**(7703):43–49. https://doi.org/10.1038/s41586-018-0063-9

Werner S, Bartrina I, Schmülling T. Cytokinin regulates vegetative phase change in *Arabidopsis thaliana* through the miR172/TOE1-TOE2 module. Nat Commun. 2021:**12**(1):5816. https://doi.org/10.1038/s41467-021-26088-z

Werner T, Köllmer I, Bartrina I, Holst K, Schmülling T. New insights into the biology of cytokinin degradation. Plant Biol (Stuttg). 2006:**8**(3):371–381. https://doi.org/10.1055/s-2006-923928

Worthen JM, Yamburenko MV, Lim J, Nimchuk ZL, Kieber JJ, Schaller GE. Type-B response regulators of rice play key roles in growth, development and cytokinin signaling. Development 2019:**146**:dev174870. https://doi.org/10.1242/dev.174870

Wulfetange K, Lomin SN, Romanov GA, Stolz A, Heyl A, Schmülling T. The cytokinin receptors of Arabidopsis are located mainly to the endoplasmic reticulum. Plant Physiol. 2011:**156**(4):1808–1818. https://doi.org/10.1104/pp.111.180539

Xie M, Chen H, Huang L, O'Neil RC, Shokhirev MN, Ecker JR. A B-ARR-mediated cytokinin transcriptional network directs hormone cross-regulation and shoot development. Nature Commun. 2018:**9**(1):1604. https://doi.org/10.1038/s41467-018-03921-6

Yamburenko MV, Worthen JM, Zeenat A, Azhar BJ, Swain S, Couitt AR, Shakeel SN, Kieber JJ, Schaller GE. Functional analysis of the rice type-B response regulator RR22. Front Plant Sci. 2020:**11**:577676. https://doi.org/10.3389/fpls.2020.577676

Yanai O, Shani E, Dolezal K, Tarkowski P, Sablowski R, Sandberg G, Samach A, Ori N. *Arabidopsis* KNOXI proteins activate cytokinin biosynthesis. Curr Biol. 2005:**15**(17):1566–1571. https://doi.org/10.1016/j.cub.2005.07.060

Yang J, Cho LH, Yoon J, Yoon H, Wai AH, Hong WJ, Han M, Sakakibara H, Liang W, Jung KH, et al. Chromatin interacting factor OsVIL2 increases biomass and rice grain yield. Plant Biotechnol. J. 2019:**17**(1):178–187. https://doi.org/10.1111/pbi.12956

Yoo SD, Cho YH, Sheen J. Arabidopsis mesophyll protoplasts: a versatile cell system for transient gene expression analysis. Nat Protoc. 2007:**2**(7):1565–1572. https://doi.org/10.1038/nprot.2007.199

Yoshida A, Ohmori Y, Kitano H, Taguchi-Shiobara F, Hirano HY. *ABERRANT SPIKELET AND PANICLE1*, encoding a TOPLESS-related transcriptional co-repressor, is involved in the regulation of meristem fate in rice. Plant J. 2012:**70**(2):327–339. https://doi.org/10.1111/j.1365-313X.2011.04872.x

Yoshida A, Sasao M, Yasuno N, Takagi K, Daimon Y, Chen R, Yamazaki R, Tokunaga H, Kitaguchi Y, Sato Y, et al. *TAWAWA1*, a regulator of rice inflorescence architecture, functions through the suppression of meristem phase transition. Proc Natl Acad Sci USA. 2013:**110**(2):767–772. https://doi.org/10.1073/pnas.1216151110

Zafar SA, Patil SB, Uzair M, Fang J, Zhao J, Guo T, Yuan S, Uzair M, Luo Q, Shi J, et al. *DEGENERATED PANICLE AND PARTIAL STERILITY 1* (*DPS1*) encodes a cystathionine β-synthase domain containing protein required for anther cuticle and panicle development in rice. New Phytol. 2020:**225**(1):356–375. https://doi.org/10.1111/nph.16133

Zhang D, Yuan Z. Molecular control of grass inflorescence development. Annu Rev Plant Biol. 2014:**65**(1):553–578. https://doi.org/10.1146/annurev-arplant-050213-040104

Zhang TQ, Lian H, Zhou CM, Xu L, Jiao Y, Wang JW. A two-step model for de novo activation of *WUSCHEL* during plant shoot regeneration. Plant Cell. 2017a:**29**(5):1073–1087. https://doi.org/10.1105/tpc.16.00863

Zhang L, Yu H, Ma B, Liu G, Wang J, Wang J, Gao R, Li J, Liu J, Xu J, et al. A natural tandem array alleviates epigenetic repression of *IPA1* and leads to superior yielding rice. Nature Commun. 2017b:**8**(1):14789. https://doi.org/10.1038/ncomms14789

Zubo YO, Blakley IC, Yamburenko MV, Worthen JM, Street IH, Franco-Zorrilla JM, Zhang W, Hill K, Raines T, Solano R, et al. Cytokinin induces genome-wide binding of the type-B response regulator ARR10 to regulate growth and development in *Arabidopsis*. Proc Natl Acad Sci USA. 2017:**114**(29):E5995–E6004. https://doi.org/10.1073/pnas.1620749114

Zürcher E, Tavor-Deslex D, Lituiev D, Enkerli K, Tarr PT, Müller B. A robust and sensitive synthetic sensor to monitor the transcriptional output of the cytokinin signaling network in planta. Plant Physiol. 2013:**161**(3):1066–1075. https://doi.org/10.1104/pp.112.211763